RSC Advances

PAPER

Check for updates

Cite this: *RSC Adv.*, 2024, **14**, 1838

Synthesis, molecular docking analysis and *in vitro* evaluation of new heterocyclic hybrids of 4-aza-podophyllotoxin as potent cytotoxic agents†

Ha Thanh Nguyen,[*ab] Ket Tran Van,[bd] Hai Pham-The,[c] Julien Braire,[e] Phuong Hoang Thi,[a] Tuan Anh Nguyen,[a] Quynh Giang Nguyen Thi,[a] Tuyet Anh Dang Thi,[ab] Giang Le-Nhat-Thuy,[ab] Tu Anh Le Thi,[a] Doan Vu Ngoc[d] and Tuyen Nguyen Van[ab]

Received 30th October 2023
Accepted 27th December 2023

DOI: 10.1039/d3ra07396c

rsc.li/rsc-advances

Two different synthetic approaches to novel heterocyclic hybrid compounds of 4-azapodophyllotoxin were investigated. The obtained products were characterized by infrared spectroscopy, nuclear magnetic resonance spectroscopy, and high-resolution mass spectrometry. MTT protocol was then performed to examine the cytotoxic activity of these products against KB, HepG2, A549, MCF7, and Hek-293 cell lines. The cytotoxic assessment indicated that all products displayed moderate to high cytotoxicity against all tested cancer cell lines. The most active compound **13k** containing the 2-methoxypyridin-4-yl group exhibited selective cytotoxicity against KB, A549, and HepG2 cell lines with the IC_{50} values ranging from 0.23 to 0.27 μM, which were between 5- to 10-fold more potent than the positive control ellipticine. Compounds **13a** (HetAr = thiophen-3-yl) and **13d** (HetAr = 5-bromofuran-2-yl) displayed high cytotoxic selectivity for A549 and HepG2 cancer cell lines when compared to the other cancer cell lines and low toxicity to the normal Hek-293 cell line. Molecular docking study was conducted to evaluate the interaction of new synthesized compounds with the colchicine-binding-site of tubulin. Besides that, physicochemical and pharmacokinetic properties of the most active compounds **13h,k** were predicted.

Introduction

Heterocycles, a class of cyclic organic compounds containing at least one ring hetero atom, have played an important role in pharmaceutical development due to their variety of biological activities such as anti-fungal,[1] antimicrobial,[2] anti-inflammatory,[3,4] anti-diabetic,[5] cytotoxic,[6,7] anti-tumor, anti-cancer,[8,9] anti-viral,[10] acetylcholinesterase inhibitory,[11] and SARS-CoV2 inhibitory activities.[12] To date, heterocycles have presented themselves as the basic core of most marketed drugs. For examples, pyridine, a nitrogen-based heterocycle, has been known as the structural unit of several targeted cancer drugs such as sorafenib,[13] regorafenib,[14] and crizotinib.[15] Ritonavir (**1**), a sulfur-based heterocycle drug, is an FDA-approved HIV protease inhibitor which can act as a potential cancer therapeutic agent (Fig. 1).[16,17] Amiodarone (**2**), a benzofuran derivative, is an antiarrhythmic medication used in the treatment of heart rate problems, ventricular fibrillation and ventricular tachycardia (Fig. 1).[18] The FDA has approved Jelmyto (mitomycin C, **3**), a pyrrole-fused quinone molecule, for treatment of adult patients with low-grade upper tract urothelial cancer (Fig. 1).[19] The quinone moiety of mitomycin C is enzymatically reduced into an active hydroquinone intermediate, which has an extraordinary ability to crosslink DNA with high efficiency.[20] Owing to the significant role of heterocyclic ring systems in drug discovery and development, many studies have been undertaken to develop biologically active heterocyclic compounds.[21–29]

Podophyllotoxin, an important plant-derived natural product, has several semisynthetic derivatives such as etoposide, teniposide and etophos, which have been employed in chemotherapy for various cancer types.[30] Although podophyllotoxin and its derivatives have been known as tubulin polymerization or DNA topoisomerase II inhibitors, they are too toxic for therapeutic use and causes some side effects. To overcome such problems, great interest has been paid to the synthesis of 4-azapodophyllotoxin derivatives in order to obtain the new anticancer agents with little side effects (Fig. 2). 4-Aza-

[a]*Institute of Chemistry, Vietnam Academy of Science and Technology, 18 Hoang Quoc Viet, Cau Giay, Hanoi, Vietnam. E-mail: hathanhnguyen1512@gmail.com*
[b]*Graduate University of Science and Technology, Vietnam Academy of Science and Technology, 18 Hoang Quoc Viet, Cau Giay, Hanoi, Vietnam*
[c]*University of Science and Technology of Hanoi, Vietnam Academy of Science and Technology, 18 Hoang Quoc Viet, Cau Giay, Hanoi, Vietnam*
[d]*Military Technical Academy, 236 Hoang Quoc Viet, Bac Tu Liem, Hanoi, Vietnam*
[e]*Université de Rennes 1, 2 Av. du Professeur Léon Bernard, 35042 Rennes, France*

† Electronic supplementary information (ESI) available. See DOI: https://doi.org/10.1039/d3ra07396c

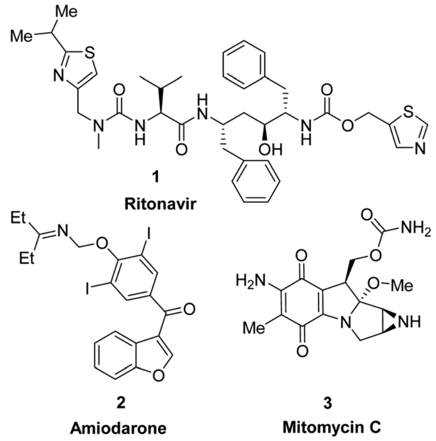

Fig. 1 Chemical structure of FDA approved drugs containing heterocyclic ring system.

podophyllotoxins have exhibited a broad spectrum of biological activities including cancer cell growth inhibition,[31] caspase-3 dependent apoptosis,[32] cell cycle arrest in the G2/M phase,[33] inhibition of tubulin polymerization and cellular microtubule disassembly[34–36] and vascular disruption effect.[37] Several hybrid compounds of 4-aza-podophyllotoxin with heterocycles have been developed and evaluated the anticancer activity.[38–41] For instance, Kamal *et al.*, has prepared a series of 4-aza-podophyllotoxin with heterocycles including benzothiazole-podophyllotoxin hybrids **6**, pyrimidine-podophyllotoxin hybrids **7**, and, indole-podophyllotoxin hybrids **8** which have inhibited tubulin polymerization, induced cell cycle arrest at G2/M phase and caspase-3 dependent apoptotic cell death in non-small lung A549 cell line.[33] Pyrazole-podophyllotoxin hybrids which have been synthesized by Magedov *et al.*, have showed apoptosis induction in cancerous Jurkat cells even after a short 24 h exposure. Azaanthraquinone-podophyllotoxin hybrids **11**, which have been designed by replacing of γ-butyrolactone ring D of 4-aza-podophyllotoxin with naphthoquinone, have exhibited medium cytotoxic activity against hepatoma carcinoma HepG2 and Hela cell lines.[42] Interestingly, azaanthraquinone-podophyllotoxin hybrids **12**, reported in our previous study,[43,44] have possessed excellent cytotoxic activity against hepatoma carcinoma HepG2 and non-small lung SK-Lu-1 cell lines with IC_{50} < 0.04 μM (Fig. 2). Hybrid compounds **12** were demonstrated to exhibit cytotoxicity by inducing cell cycle arrest at G2/M phase, activating caspase-3/7 activation, and promoting apoptosis in a concentration-dependent manner. In spite of the many researches focused on the synthesis of aza-podophyllotoxin hybrids, the replacement of ring E with heterocycles has not attracted enough attention so far. Accordingly, in the view of the above mentioned facts and as a continuation of our efforts on the synthesis of biologically active compounds,[45–49] herein, we have focused our research interest toward the synthesis of novel azaanthraquinone-podophyllotoxin hybrids with heterocyclic ring E **13** *via*

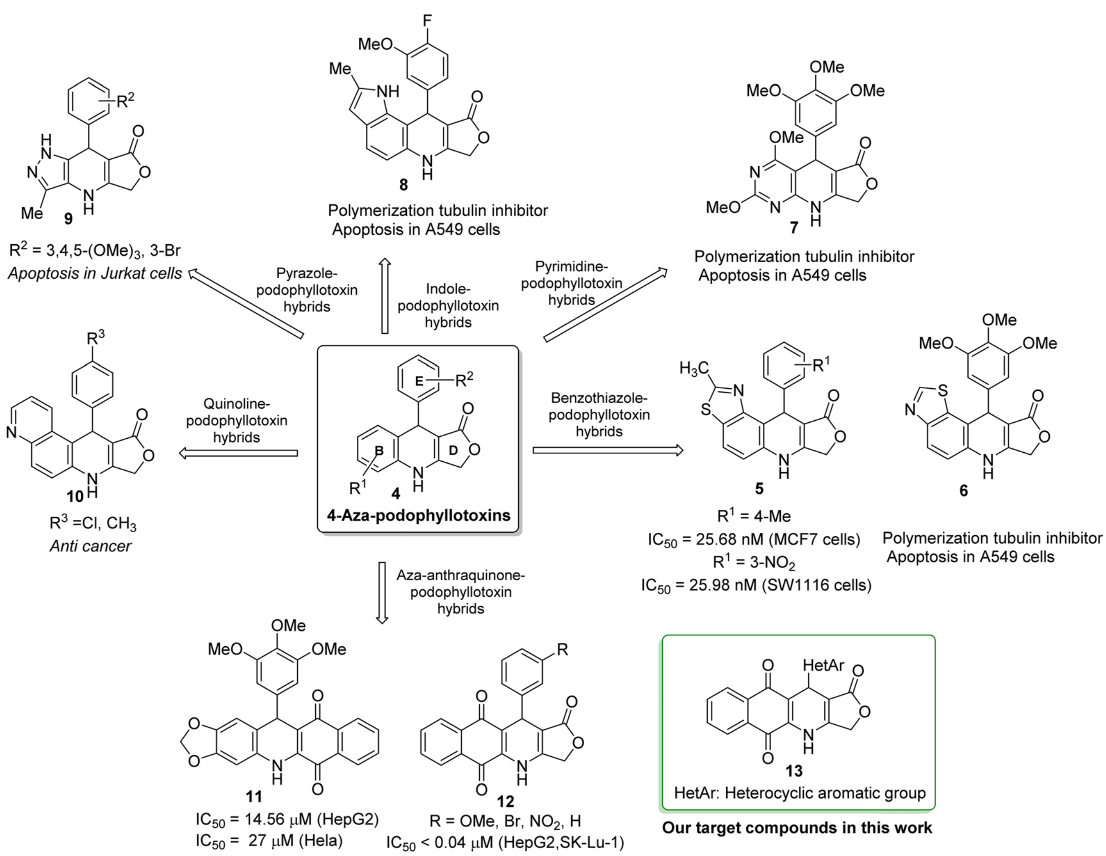

Fig. 2 Hybrid compounds of 4-aza-podophyllotoxin with heterocycles.

microwave-assisted multicomponent reactions (Fig. 2), and evaluation of their cytotoxic activity against various cancer cell lines by using MTT colorimetric method. Besides, synthesized compounds **13** were docked into the binding sites of colchicine in tubulin and their binding energies as well as physicochemical and pharmacokinetic properties were determined.

Results and discussion

Chemistry

Two convenient multicomponent synthetic approaches have been adopted to synthesize the target compounds **13** (Scheme 1). In the approach A, a range of structurally diverse heteroaromatic aldehydes **16** was subjected to the four-component reactions with 2-hydroxy-naphthoquinone (**14**), tetronic acid (**15**) and ammonium acetate (**17**) in glacial acetic acid (gl. AcOH) at 120 °C in 20 min under microwave irradiation, leading to products **13** in low yield ranging from 20 to 34% (Table 1). The formation of products **13** possibly started from Knoevenagel condensation of 2-hydroxy-1,4-naphthoquinone (**14**) with aldehydes, followed by Michael addition to 4-aminofuran-2(5*H*)-one **19**, produced from the reaction of tetronic acid **15** with ammonia. The adduct **21** underwent tautomerization, intramolecular cyclization and dehydration to form products **13** (Scheme 2).

In the approach B, three-component synthesis of target products **13** from 2-amino-naphthoquinone, heteroaromatic aldehydes, and tetronic acid was investigated. In our preliminary studies, we indicated that the use of *p*-toluenesulfonic acid (*p*-TsOH) as an acid catalyst and gl. AcOH as a solvent promoted the three-component reactions to generate products in higher yields. Thus, *p*-TsOH (20 mol%) was supplemented to the reaction mixtures in gl. AcOH, and the reactions were then stirred at 120 °C, under microwave irradiation (150 W). The reactions proceeded rapidly to completion within 20 min. As shown in Table 1, under these optimized conditions, products **13** were afforded in good yields (60–74%). The synthetic approaches proceeded *via* a sequential steps including Knoevenagel condensation of 2-amino-1,4-naphthoquinone (**14**) with heteroaromatic aldehydes, Michael addition to tetronic acid, tautomerization, intramolecular cyclization and dehydration (Scheme 2).

It is worth mentioning that the approach B (synthesis by three-component reactions) is likely to be more efficient for the synthesis of target products **13** in comparison with the approach A (synthesis by four-component reactions). In approach B, the effect of heterocyclic substituents on aldehyde on the outcome of reactions could be observed more clearly. For instance, pyridinecarboxaldehyde derivatives **16k–m** displayed the highest reactivity to give the desired products **13k–m** in high yield (72–74%). The fusion of a benzene ring with five-membered aromatic heterocyclic ring of aldehydes improved the reaction yields compared to five-membered heterocyclic aldehydes. Benzo[*b*]thiophene-3-carbaldehyde (**16e**) furnished 70% yield of the product **13c**, whereas, thiophene-3-carbaldehyde (**16a**) afforded **13a** in 64% yield.

The structure of obtained compounds were examined by IR, ^{1}H and ^{13}C NMR, HSQC, HMBC, DEPT, and HRMS. Compound **13a** was focused for illustrating the ^{1}H and ^{13}C assignments. In general, the ^{1}H-NMR spectrum of **13a**, presented a typical singlet at δ_H 10.60 ppm corresponding to an –NH group, two doublets of doublets at δ_H 8.05 (1H, dd, $J = 1.2$, 7.8 Hz, H6), and 7.93 (1H, dd, $J = 0.6$, 7.8 Hz, H9), two triples of doublets at δ_H 7.85 (1H, td, $J = 1.2$, 7.2 Hz, H8), 7.81 (1H, td, $J = 1.2$, 7.2 Hz, H7) corresponding to four aromatic protons in naphthoquinone ring. Three aromatic protons in thiophene ring appeared at δ_H 7.38 (1H, dd, $J = 3.0$, 4.8 Hz, H-5′), 7.24 (1H, dd, $J = 0.6$, 3.0 Hz, H-2′), 7.07 (1H, dd, $J = 1.2$, 4.8 Hz, H-4′). Moreover, the typical singlet at 5.11 ppm was referred to the H-11 proton, two doublets were observed at 4.94 ppm and 4.90 ppm with a coupling constant of 16.8 Hz assignable to the 3-CH_2 protons in γ-butyrolactone ring. On the other hand, the ^{13}C NMR spectrum of product **13a** displayed 19 carbon resonances, which were fully assigned with DEPT, ^{1}H–^{13}C HSQC and ^{1}H–^{13}C HMBC support. The DEPT-135 shows 8 positive peaks and 1 negative peak. The negative peak at 66.1 ppm corresponded to methylene (CH_2) carbon C-3. Proton signal (H-11) at 5.11 ppm showed proton-carbon couplings to C-10 at 182.1 ppm, C-1 at 171.2 ppm, C-3a at 156.1 ppm, C-4a at 139.2 ppm, C-3′ at 145.0 ppm, C-4′ at 127.7 ppm, C-2′ at 122.4 ppm, C-10a at 118.0 ppm, and C-11a at 101.6 ppm (Fig. 3). Moreover, under positive HR–ESI–MS conditions, $[M + H]^+$ at *m/z* 350.0484, which confirms the molecular formula for compound **13a** is $C_{19}H_{11}NO_4S$.

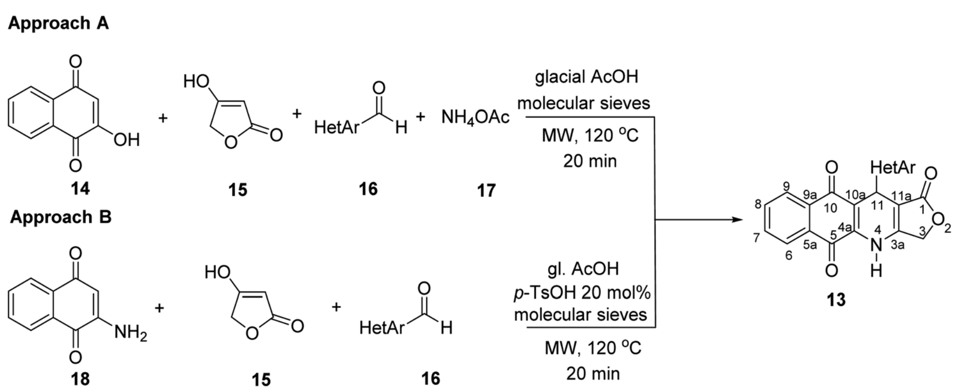

Scheme 1 Synthesis of compounds **7** under microwave irradiation.

Table 1 Synthesis of compounds 13 under microwave irradiation

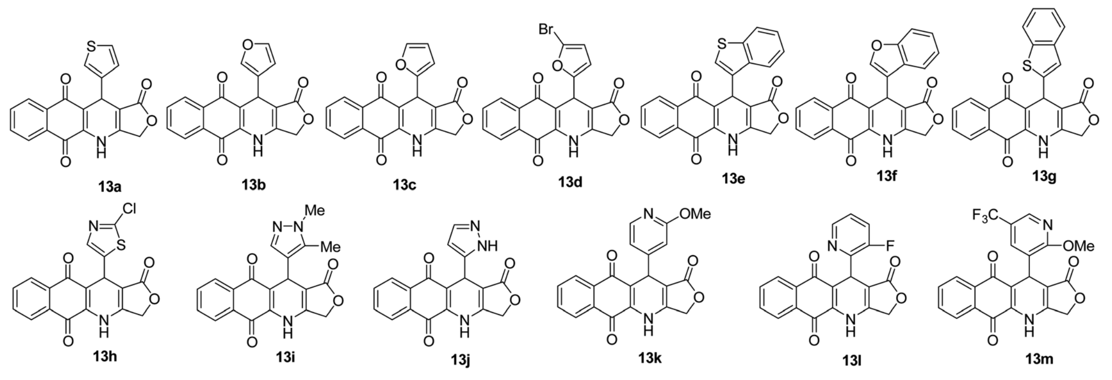

Entry	Product	Yield (%) Approach A	Yield (%) Approach B
1	**13a**	29	64
2	**13b**	25	62
3	**13c**	20	60
4	**13d**	20	62
5	**13e**	33	70
6	**13f**	32	68
7	**13g**	33	69
8	**13h**	28	64
9	**13i**	27	63
10	**13j**	20	61
11	**13k**	34	74
12	**13l**	32	72
13	**13m**	33	72

Cytotoxicity of synthesized compounds

All of these products were further studied cytotoxicity evaluation *in vitro* against cultured A549 (human lung adenocarcinoma), MCF7 (human breast adenocarcinoma), KB (human mouth epidermal carcinoma), HepG2 (human hepatocellular carcinoma) and Hek-293 (human embryonic kidney

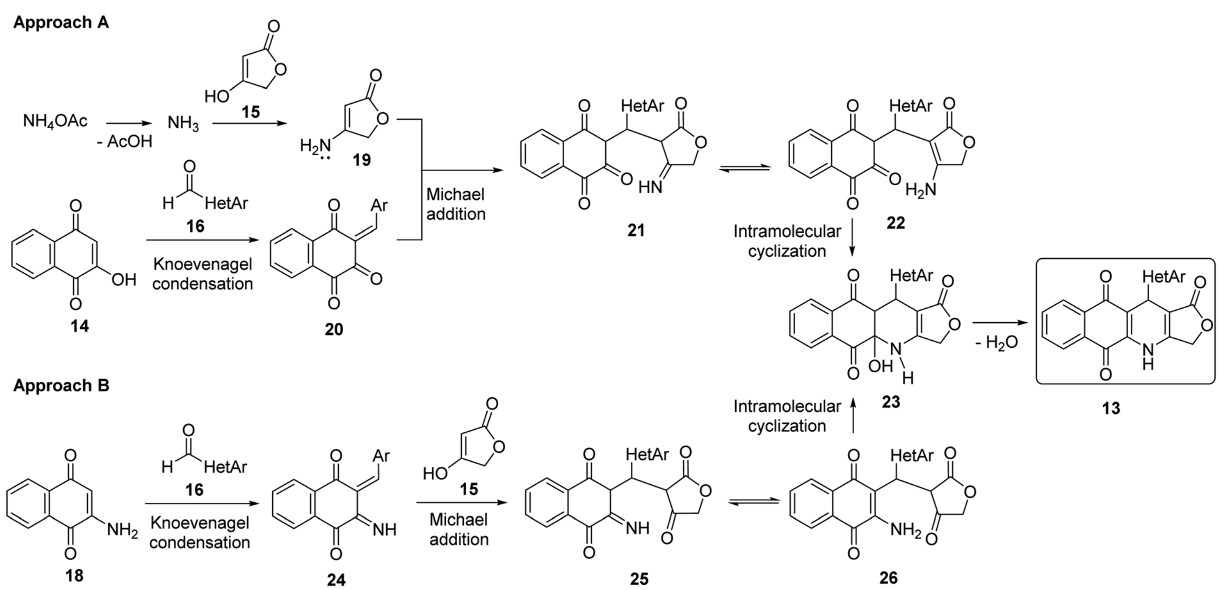

Scheme 2 Plausible mechanism for the formation of obtained products 13.

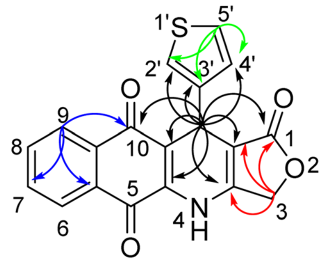

Fig. 3 Key correlations of protons H-11 (black arrows), H-3 (red arrows), H-9 (blue arrows), and H-5′ (green arrows) in ^{1}H–^{13}C HMBC spectrum of compound **13a**.

293) cell lines, in comparison to ellipticine, the positive control, by using MTT assay (Table 2). The selective index (SI) of products was calculated as the ratio of the IC_{50} value in Hek-293 (human embryonic kidney 293) cell line to the IC_{50} value in cancer cell line (Table 3). As illustrated in Table 2, all products showed high and moderate cytotoxic activity to all tested cancer cell lines with IC_{50} values ranging from 0.16 to 14.22 μM. Cytotoxic activity of compounds **13a,h,k** was better than that of ellipticine against 4 tested cancer cell lines, a fact supporting their anti-cancer activity. Besides, products **13f** (HetAr = benzofuran-3-yl) exerted almost 1.8-fold higher toxicity to KB and HepG2 cells when compared with ellipticine. Notably, product **13k** (HetAr = 2-methoxypyridin-4-yl) exhibited the significantly potent and selective cytotoxicity against KB, A549, and HepG2 cell lines with the IC_{50} values ranging from 0.23 to 0.27 μM. The cytotoxic activity of product **13k** toward KB, A549, and HepG2 cancer cells was approximately 10 times higher in relation to normal Hek-293 cells (Table 3). Product **13h** (HetAr = 2-chlorothiazol-5-yl) showed the highest growth inhibitory activity against A549 and MCF7 cancer cell lines and normal Hek-293 cells with IC_{50} values of 0.16, 1.07, and 1.38 μM, respectively. Compound **13a** (HetAr = thiophen-3-yl) displayed higher cytotoxic selectivity for A549 cancer cells when compared to the other cancer cell lines and low toxicity to normal Hek-293 cell line with IC_{50} = 22.90 μM, what can indicate their specificity to cancer cell lines. In particularly, compound **13d** (HetAr = 5-bromofuran-2-yl) exhibited selective cytotoxicity against HepG2 cancer cells with IC_{50} value of 0.30 μM, which was 122-fold higher than its IC_{50} value for Hek-293 cells (Table 3).

Molecular docking study

Based on experimental assessments, it can be initially identified that compounds **13a–13m** are good cytotoxic agents. Due to crucial function in mitosis and cell division, microtubules, which are produced through the polymerization of heterodimers of α and β-tubulins, have been a desirable target in the development of novel anticancer medicines.[50] Meanwhile, podophyllotoxin has long been regarded as a potent microtubule destabilizing agent that binds to the tubulin colchicine site, inhibiting tubulin polymerization and suppressing the production of microtubules.[44,51] Therefore, in this study, we used molecular docking to evaluate the interaction of novel synthesized substances with this molecular target. The natural tubulin substrate colchicine will be used as a positive control.

Table 3 Selective index for active compounds

		Selective index			
Entry	Compound	KB	A549	HepG2	MCF7
1	**13a**	16.00	47.90	16.00	11.12
3	**13b**	1.37	4.47	1.12	1.09
4	**13c**	1.02	4.75	3.88	1.20
5	**13d**	13.19	18.00	122.40	3.58
6	**13e**	1.02	1.12	1.07	0.85
7	**13f**	17.98	2.81	15.10	1.56
8	**13g**	1.31	4.18	1.03	1.16
9	**13h**	1.23	8.55	1.71	1.29
10	**13i**	1.14	5.40	1.57	1.18
11	**13j**	0.63	0.69	0.86	1.16
12	**13k**	9.30	9.30	10.81	1.86
13	**13l**	2.18	4.74	1.85	1.39
14	**13m**	3.61	5.92	2.87	2.31
15	Ellipticine	2.88	3.94	2.65	2.68

Table 2 Cytotoxicity of the products **7** against KB, HepG2, A549, MCF7, and Hek-293 cell lines

	IC_{50}, μM				
Product	KB	A549	HepG2	MCF7	Hek-293
13a	1.43 ± 0.14	**0.48 ± 0.03**	1.43 ± 0.15	2.06 ± 0.66	22.90 ± 2.18
13b	10.05 ± 1.17	3.09 ± 0.39	12.36 ± 1.29	12.63 ± 1.14	13.80 ± 1.41
13c	14.22 ± 1.23	3.06 ± 0.27	3.75 ± 0.69	12.15 ± 1.14	14.55 ± 1.35
13d	2.81 ± 0.32	2.06 ± 0.22	**0.30 ± 0.06**	10.36 ± 1.29	37.12 ± 3.30
13e	10.94 ± 1.40	9.94 ± 0.73	10.42 ± 1.18	13.07 ± 1.60	11.17 ± 0.85
13f	1.10 ± 0.09	7.02 ± 0.91	1.30 ± 0.13	12.65 ± 1.20	19.69 ± 1.70
13g	9.94 ± 0.65	3.13 ± 0.20	12.67 ± 1.40	11.27 ± 1.78	13.07 ± 1.70
13h	1.12 ± 0.10	**0.16 ± 0.02**	**0.81 ± 0.11**	**1.07 ± 0.10**	1.38 ± 0.18
13i	10.74 ± 1.27	2.27 ± 0.22	7.80 ± 0.53	10.41 ± 0.80	12.26 ± 1.13
13j	6.00 ± 0.63	5.43 ± 0.39	4.35 ± 0.57	3.24 ± 0.36	3.75 ± 0.69
13k	**0.27 ± 0.24**	**0.27 ± 0.21**	**0.23 ± 0.02**	1.34 ± 0.16	2.48 ± 0.32
13l	4.69 ± 0.58	2.15 ± 0.25	5.52 ± 0.86	7.34 ± 0.94	10.21 ± 1.24
13m	4.63 ± 1.04	2.83 ± 0.54	5.83 ± 0.86	7.26 ± 1.29	16.73 ± 1.94
Ellipticine	1.95 ± 0.12	1.42 ± 0.08	2.11 ± 0.16	2.09 ± 0.16	5.60 ± 0.37

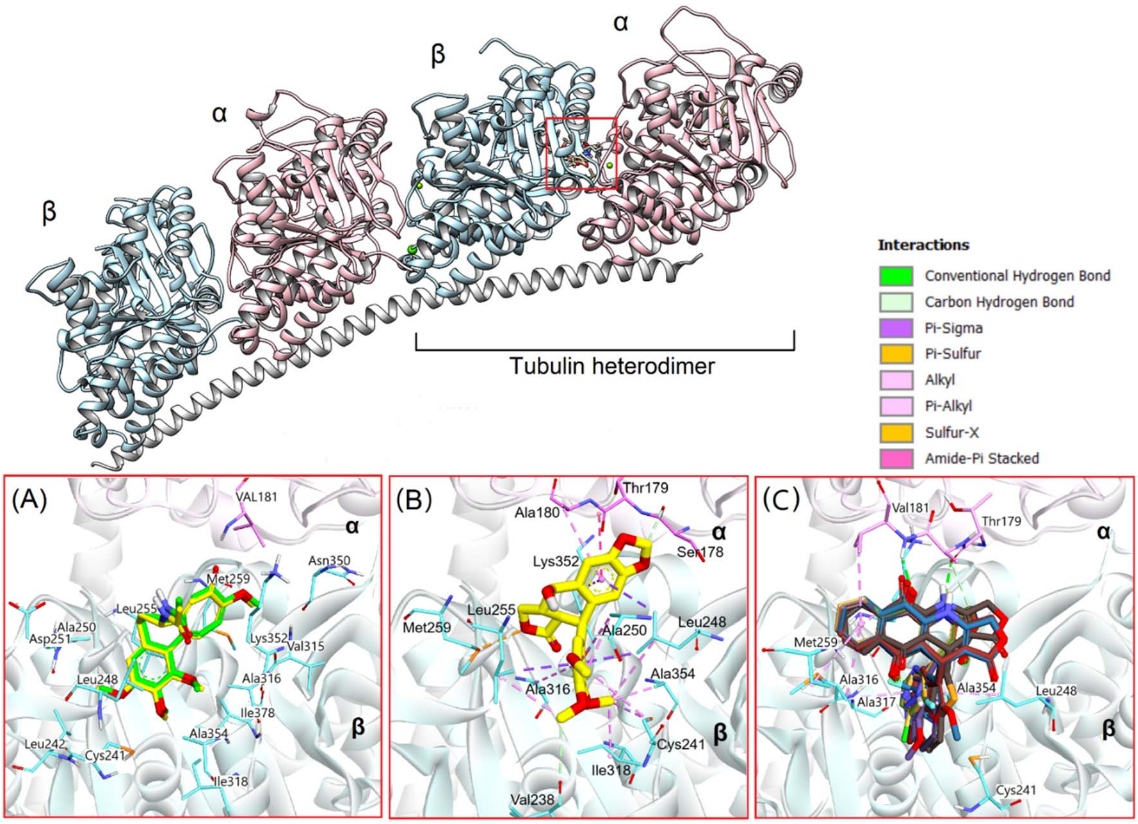

Fig. 4 (A) Redocked poses (green) and original poses (yellow) of colchicine in tubulin; (B) docking pose of podophyllotoxin, and (C) docking poses of 13 synthesized compounds in colchicine binding site.

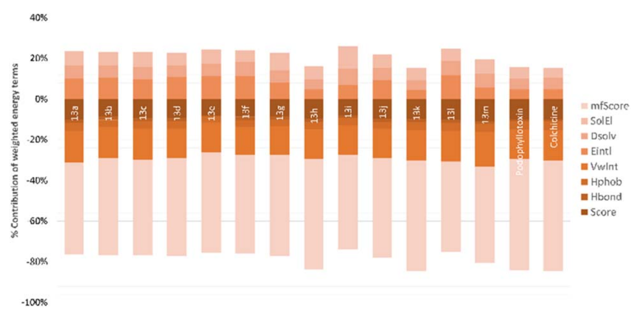

Fig. 5 Contribution (%) of the different energy terms to the binding affinity (score) of tubulin-ligands: the van der Waals interaction energy (VwInt), Hydrogen Bond energy (Hbond), the hydrophobic energy (Hphob), internal conformation energy (Eintl), the desolvation of exposed H-bond donors and acceptors (Dsolv), the solvation electrostatics energy change upon binding (SolEl), the potential of mean force score (mfScore).

Firstly, colchicine were redocked into the active site in tubulin to validate the docking process. As the results, the redocked conformers tightly bound to the colchicine binding site of tubulin with a very high matching with the co-crystallized structure (RMSD = 0.3339 Å). Moreover, it preserves the key interactions such as hydrogen bonds with Val181, Ala180… of the α subunit through its methoxytropone ring, hydrophobic interactions with Leuβ242, Cysβ241, Alaβ354, and Alaβ316 (Fig. 4A),[52] suggesting the validity of established docking protocol.

In the next step, podophyllotoxin, which is considered reference compound was also docked into the binding site of tubulin. The results were similar to those previously determined.[44] As can be seen in Fig. 4, this compound exhibited a large interaction network with residues in the binding site. Some of the key interactions should be mentioned here are the hydrogen bonds with Val178, Ala180… of the α subunit and numerous hydrophobic interactions with Cys241, Ala250, Leu248, Leu255, Ala354, and Ala316 of the β subunit (Fig. 4B). The binding energy was determined to be −18.68 kcal mol^{-1}, and hydrogen bonding and hydrophobic stacking interactions the most contributed components (Fig. 5). The results obtained confirmed the similarity and accuracy of the docking protocol.

After validating the docking protocol, all 13 synthesized compounds (**13a–13m**) were docked into the binding site of colchicine in tubulin, using the above validated protocol. The binding energies and the main interactions between the compounds and tubulin in comparison with podophyllotoxin are summarized in Table 4 and Fig. 4–6.

Overall, the docking results of 13 substances **13a–13m** were similar to colchicine and those previously published.[44] They are all capable of binding to the active site of colchicine in tubulin. The colchicine binding site was divided into three zones including zones 1, 2, and 3 according to Massaroti *et al.*[53] zone 1 is surrounded by the residues Valα181, Serα178, Metβ259, Asnα101, and is situated at the α subunit interface. Located in the β subunit, zone 2 is an accessory hydrophobic pocket made

Table 4 Binding energy between compounds **13a–13m** and active site of tubulin compared to co-crystallized compounds

Cpd	Binding energy (kcal mol^{-1})	Interaction with residues
13a	−16.38	H-bond: Val 181α, Thr 179α, Ala 180α Hydrophobic: Ala 354β, Leu 248β, Ala 316β, Lys 352β, Met 259β
13b	−13.79	H-bond: Val 181α, Thr 179α, Ala 180α, Ala 354β, Ala 317β Hydrophobic: Leu 248β, Ala 316β, Lys 352β, Met 259β
13c	−14.55	H-bond: Val 181α, Thr 179α, Ala 180α Hydrophobic: Ala 354β, Leu 248β, Ala 316β, Lys 352β, Met 259β
13d	−15.29	H-bond: Val 181α, Thr 179α, Ala 180α Hydrophobic: Ala 354β, Leu 248β, Ala 316β, Lys 352β, Met 259β, Ile 318β, Cys 241β
13e	−14.09	H-bond: Val 181α, Thr 179α, Ala 180α Hydrophobic: Ala 354β, Leu 248β, Ala 316β, Lys 352β, Met 259β, Leu 255β, Cys 241β
13f	−16.45	H-bond: Val 181α, Thr 179α, Ala 180α, Asn 101α, Leu 255β, Ala 250β Hydrophobic: Ala 354β, Leu 248β, Ala 316β, Lys 352β, Met 259β, Leu 255β, Asn 258β, Ala 250β
13g	−15.08	H-bond: Val 181α, Thr 179α, Ala 180α, Leu 255β, Lys 352β Hydrophobic: Ala 354β, Leu 248β, Ala 316β, Lys 352β, Met 259β, Leu 255β, Asn 258β, Ala 250β, Cys 241β
13h	−17.86	H-bond: Val 181α, Thr 179α, Ala 180α Hydrophobic: Ala 354β, Leu 248β, Ala 316β, Lys 352β, Met 259β, Ile 318β, Cys 241β
13i	−13.83	H-bond: Val 181α, Ala 180α, Asn 101α, Ala 317β Hydrophobic: Ala 354β, Leu 248β, Leu 255β, Ala 316β, Lys 352β, Met 259β, Ile 318β
13j	−15.64	H-bond: Val 181α, Thr 179α, Ala 180α, Ala 317β, Lys 352β Hydrophobic: Ala 354β, Leu 248β, Ala 316β, Lys 352β, Met 259β
13k	−18.45	H-bond: Val 181α, Thr 179α, Ala 180α, Ala 317β Hydrophobic: Ala 354β, Leu 248β, Ala 316β, Lys 352β, Met 259β, Ile 318β, Cys 241β
13l	−15.78	H-bond: Val 181α, Thr 179α, Ala 180α, Ala 317β, Lys 352β Hydrophobic: Ala 354β, Leu 248β, Ala 316β, Lys 352β, Met 259β
13m	−16.8	H-bond: Val 181α, Ala 180α, Ala 317β, Ala 316β, Asn 101α, Asp251β, Ala 250β Hydrophobic: Ala 354β, Leu 248β, Ala 316β, Lys 352β, Met 259β, Leu255β, Thr 353β
Podophylotoxin	−18.68	H-bond: Ser 178α, Ala 180α, Ala 317β, Ala 316β, Asn 101α, Asp251β, Ala 250β Hydrophobic: Val 238β, Cis 241β, Leu 248β, Ala 316β, Ala 318β, Lys 352β, Met 259β, Leu255β, Thr 353β
Colchicin	−19.18	H-bond: Val 181α, Ala 180α, Ala 250β, Asp251β, val 315β, asn 350β Hydrophobic: Leu 255β, Leu 248β, Leu 242β, Cys 241β, Ile 318β, Ala 354β, Ile 378β, Ala 316β, Met 359β, Lys 352β

up of the residues Lysβ352, Valβ318, Alaβ317, Alaβ316, Leuβ255, Alaβ250, Leuβ248, Leuβ242, and Cysβ241 zone 3, which is buried deeper inside the β subunit, is formed by the residues Thrβ239, Valβ238, Tyrβ202, Gluβ200, Pheβ169, Asnβ167, Glnβ136, and Ileβ4… Therein, these studied conformations with rigid structures are capable of stretching into the deeper zone 2 of the β-subunit.[54] Almost all the synthesized compounds conserved these key interactions such as the hydrogen bond between the carbonyl group of the quinone ring and Valα181, Alaα180; the hydrophobic interactions which are mainly pi-alkyl stacking with most residues of zone 2 like Lysβ352, Alaβ317, Alaβ316, Leuβ255, Alaβ250, and so on. Moreover, all compounds formed hydrogen bonds between N and Thrα179 that do not exist in colchicine,[52] making it bind to the active site more strongly.

The docking poses and binding energies also showed good ability to discriminate the good ligands from the bad ones. **13b** and **13c** were determined to be two of the weakest ligands of tubulin. As can be seen in Fig. 6, these compounds were quite different from **13k** and **13h** in alignment with podophyllotoxin. In fact, fewer interactions were observed in **13b** and **13c**, being several stacking interactions with HetAr with residues in the β subunit, such as Asn101, Ala250, Leu248, and Ala316 the most important ones. In particular, the orientation of HetAr in **13b** and **13c** were different from **13k** and **13h**, suggesting the change in their target interactions.

The relative binding energies were determined based on a GBSA/MM-type function implemented into ICM pro.[66] In addition, other energy terms extracted from the final complex, including Hbond, Vwin. Accordingly, compound **13k** has the strongest binding energy at −18.05 kcal mol^{-1}. Besides general interactions, it also formed hydrogen bonds between the lactone ring and Asn101α of zone 1, and between the carbonyl group of the quinone ring and Leuβ255 of zone 2. Additionally, it interacts better with more residues of zone 2 of colchicine binding site through its substituent. Compound **13h** had good binding energy of −17.86 kcal mol^{-1} resulted by key hydrogen bonds with residues of zone 1 and hydrophobic interactions which are similar to compound **13k** (Fig. 6). The results also highlighted the highest values of Hbond and Hphob energies of **13h** and **13k** compared to the other derivatives, which correlated well with the order ranking of all the compounds (Fig. 5). There is a concurrence between the binding energy and the ICM docking mfScore which refers to the strength of the inhibitor–tubulin interaction. The mfScore values of **13h** and **13k** were −102.91 and −103.1 kcal mol^{-1}, which are similar to podophyllotoxin. Interestingly, Hbonds appear to have small impact on the binding ability of synthesized compounds. While hydrogen bonding energies of **13b** and **13c** are quite high, their overall energies computed by GBSA/MM-type and mfScore functions showed significantly lower than podophyllotoxin and colchicine (see Table S1†). For the generated docking

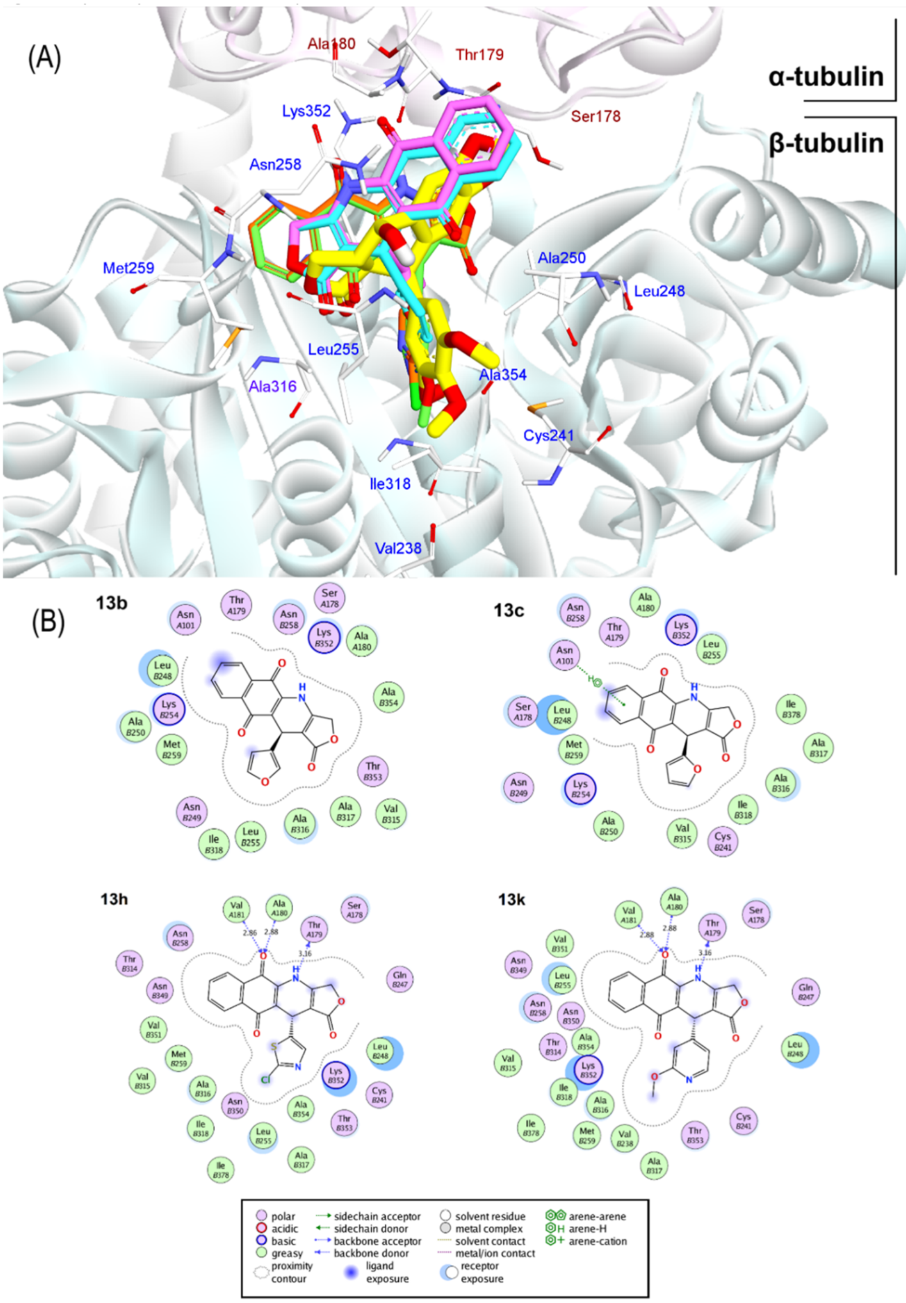

Fig. 6 (A) Superimposition of docking poses of **13b** (purple carbon), **13c** (cyan carbon), **13h** (orange carbon), and **13k** (green carbon) against podophyllotoxin (yellow carbon). (B) Topological interactions of **13b**, **13c**, **13h**, and **13k** with the residues in the active sites of α and β-tubulin domains (labeled with A and B prefixes).

conformations, the hydrophobic and van der Waals interaction appear to be the driving forces for binding ability of tested compounds. Over podophyllotoxin all, the docking results are in consistency with our previous findings, and in turn match well with experimental ranking using the cytotoxicity tests.[67,69]

Physicochemical and pharmacokinetic properties prediction

The above experimental test revealed that all 13 compounds exhibit good activity against a variety of cancer cell lines. In which, the two chemicals **13h** and **13k** have the most potential. So, we performed assessments related to physicochemical and pharmacokinetic feature as a criteria for drug-likeness evaluation.

First, radar plot of the physicochemical properties in Fig. 7 showed that both compounds met most of the criteria, excepting logP and logS. This issue may affect to their membrane permeability. However, according to the prediction of SwissADME, the $LogP_{o/w}$ value of them are less than 5.0 that is suitable for absorption.[55,56] In terms of solubility, based on ESOL topological model, they classified as moderately soluble

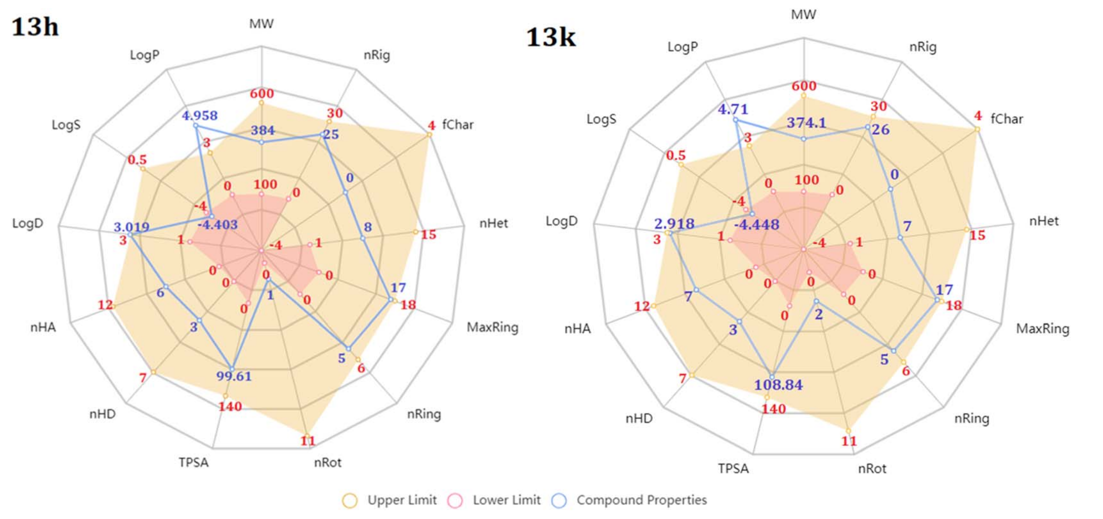

Fig. 7 Radar diagram illustrating the physicochemical characteristics of **13h** and **13k**. MW: molecular weight, nRig: number of rigid bonds, fChar: formal charge, nHet: number of heteroatoms, MaxRing: number of atoms in the biggest ring, nRing: number of rings, nRot: number of rotatable bonds, TPSA: topological polar surface area ($Å^2$), nHD: number of hydrogen bond donors, nHA: number of hydrogen bond acceptors, logD: log of octanol partition coefficient at physiological pH 7.4, logS: log of aqueous solubility (mol L^{-1}), and logP: log of octanol partition coefficient.

chemicals (Table 4). In addition, **13h** and **13k** were predicted to have zero alert according to the Pan Assay Interference Compounds (PAINS) which is desired to avoid promiscuous behavior and nonselective reactivity with proteins.

In addition, these two compounds were subjected to drug-likeness prediction. Table 5 demonstrates that **13h** and **13k** successfully accomplished all the drug-likeness rules with no violations but failed to pass lead-likeness rule due to their molecular weight.[57]

Second, the properties related to Absorption, Distribution, Metabolism and Excretion (ADME) were analyzed. According to the absorption, the predicted values showed that both

Table 5 Drug-like and pharmacokinetic properties of **13h** and **13k**

Predicted parameters	13h	13k
Drug likeness		
Lipinski	Accept	Accept
Goshe	Accept	Accept
Veber	Accept	Accept
Egan	Accept	Accept
Muegge	Accept	Accept
Bioavailability score	0.55	0.55
Lead-likeness	No, (MW > 350)	No, (MW > 350)
PAINS	0 alert	0 alert
Absorption		
Gastrointestinal absorption	High	High
Pgp-substrate	No	No
Log K_p (skin permeation)	-6.72 cm s^{-1}	-6.72 cm s^{-1}
Distribution		
Plasma protein binding	100.0% (not optimal)	97.87% (not optimal)
Volume distribution	0.402	0.413
Blood–brain barrier (BBB) penetration	No	No
Metabolism		
CYP interaction*	CYP1A2 inhibitor (0.94) CYP2C9 inhibitor (0.66)	CYP1A2 inhibitor (0.92) CYP2C9 inhibitor (0.75) CYP2D6 substrate (0.58)
Excretion		
Clearance (CL)	3.043 mL min^{-1} kg (low)	3.317 mL min^{-1} kg (low)
Half-life ($T_{1/2}$)	0.066 h (short)	0.194 (short)

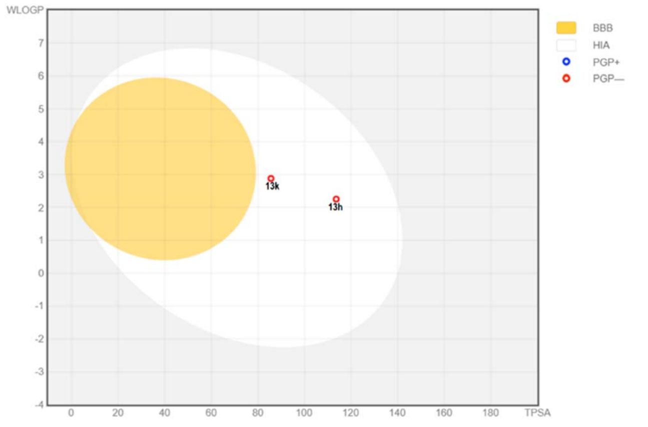

Fig. 8 BOILED-Egg diagram of two potent compounds **13h** and **13k**. Abbreviation: BBB: blood–brain barrier; HIA: human intestinal absorption; PGP+: P-glycoprotein substrate; PGP-: P-glycoprotein non-substrate.

compounds have high human intestinal absorption.[58] According to the BOILED-Egg plot (Fig. 8), they were not glycoprotein-P substrate and shas high intestinal absorption percent.[59,60] Prediction of skin permeability showed that they are less permeable across the skin. In addition, **13f** and **13h** could not across the blood–brain barrier, suggesting a little effect on the central nervous system (CNS). These compounds were estimated to have high plasma protein binding which may narrow their therapeutic index. Both compounds showed optimal volume of distribution. In accordance with the first-pass metabolism, hepatic cytochrome plays a pivotal role in catalytic reactions. Our predictions showed that **13h** and **13k** mainly interacted with CYP1A2 and CYP2C9, suggesting potential drug–drug interactions with some medications and food.[61] These compounds were also estimated to have low clearance together with a short half-life in human body.

ADMETlab 2.0 was subsequently used to anticipate toxicity of **13h** and **13k** (Table 6).[62] Accordingly, both compounds are not hERG blockers, suggesting low cardiotoxicity effect.[44] Besides, they did not show human hepatoxicity, mutagenic effect, and eye corrosion. However, **13k** may cause reactions with the skin and respiratory tract. Meanwhile **13h** showed no interaction with most organs excepting the respiratory system. In general, these derivatives provided suitable physicochemical and ADMET profiles to be considered as good anticancer compounds for further hit-to-lead optimization stages.

Experimental

Materials and methods

All chemicals were used as received without any further purification and obtained from Aldrich or Merck. Microwave irradiation experiments were performed using an Anton Paar Microwave Synthetic Reactor Monowave 400. Merck silica gel 60 F254 plates and Merck silica gel 60 (240–400 mesh) were used for thin-layer chromatography and column flash chromatography, respectively. Melting points were measured in open capillaries on a Buchi melting point B-545 apparatus (Buchi Instrument, Switzerland) and the values reported are uncorrected. A SCIEX X500 QTOF mass spectrometer in ESI (+) or ESI (−) mode was used to calculate the HRMS spectra. IR spectra have been recorded as KBr pellets, with a PerkinElmer Spectrum Two FT-IR spectrometer. NMR experiments were acquired using a Bruker Avance III spectrometer (600 and 125/150 MHz).

General procedure for synthesis of compounds 13a–m

Approach A: Under microwave irradiation (150 W), a mixture of 2-hydroxy-1,4-naphthoquinone (**14**, 1 mmol), tetronic acid (**15**, 1 mmol), heteroaromatic aldehyde (**16a–m**, 1 mmol), and NH_4OAc (**17**, 3.0 mmol) in glacial acetic acid (3 mL) was stirred for 20 min at 120 °C. The reaction mixture was then poured into water (20 mL) and extracted with dichloromethane (3 × 20 mL), washed with brine (3 × 10 mL). The combined organic layer was dried over anhydrous Na_2SO_4, concentrated *in vacuo*, and purified by column chromatography using a dichloromethane-acetone eluent (20 : 1, 25 : 2, v/v) to furnish products **13a–m**.

Approach B: Under microwave irradiation (150 W), a mixture of 2-amino-1,4-naphthoquinone (**18**, 1 mmol), tetronic acid (**15**, 1 mmol), heteroaromatic aldehyde (**16a–m**, 1 mmol), and *p*-TsOH (0.02 mmol) in glacial acetic acid (3 mL) was stirred for 20 min at 120 °C. The reaction mixture was then poured into water (20 mL), extracted with dichloromethane (3 × 20 mL), and washed with brine (3 × 10 mL). The combined organic layer was dried over anhydrous Na_2SO_4, concentrated *in vacuo*, and

Table 6 Toxicity predicted using ADMETlab 2.0 of the two most potential compounds

Toxicity[a]	13h	13k
hERG blockers	Inactive (0.002)	Inactive (0.009)
Human hepatotoxicity	Negative (0.425)	Negative (0.12)
AMES toxicity	No (0.324)	No (0.273)
Rat oral acute toxicity	No (0.412)	No (0.436)
FDA maximum (recommended) daily dose	Negative (0.11)	Negative (0.235)
Skin sensitization	No (0.497)	Yes (0.747)
Respiratory toxicity	Yes (0.687)	Yes (0.893)
Eye irritation	No (0.263)	No (0.135)

[a] The values in parentheses display the probability of being toxic.

purified by column chromatography using a dichloromethane-acetone eluent (20 : 1, 25 : 2, v/v) to furnish products **13a–m**.

11-(Thiophen-3-yl)-4,11-dihydrobenzo[*g*]furo[3,4-*b*]quinolin-1,5,10(3*H*)-trione (13a). Yield 101 mg (29% – approach A), 224 mg (64% – approach B), orange solid, mp. 298–299 °C. IR (KBr) ν_{max}/cm^{-1} 3238, 3086, 2967, 2930, 2890, 1709, 1657, 1636 1606, 1589, 1500, 1395, 1351, 1334, 1303, 1240, 1191, 1070, 1015, 932, 838, 783, 727. ^{1}H NMR (DMSO-d_6, 600 MHz): δ 10.60 (1H, s, –NH), 8.05 (1H, dd, J = 1.2, 7.8 Hz, H-6), 7.93 (1H, dd, J = 0.6, 7.8 Hz, H-9), 7.85 (1H, td, J = 1.2, 7.2 Hz, H-8), 7.81 (1H, td, J = 1.2, 7.2 Hz, H-7), 7.38 (1H, dd, J = 3.0, 4.8 Hz, H-5′), 7.24 (1H, dd, J = 0.6, 3.0 Hz, H-2′), 7.07 (1H, dd, J = 1.2, 4.8 Hz, H-4′), 5.11 (1H, s, H-11), 4.97 (1H, d, J = 16.8 Hz, H^a-3), 4.87 (1H, d, J = 16.8 Hz, H^b-3). ^{13}C NMR (DMSO-d_6, 125 MHz) δ 182.1 (C-10), 179.6 (C-5), 171.2 (C-1), 156.1 (C-3a), 145.0 (C-3′), 139.2 (C-4a), 134.9 (C-8), 133.4 (C-7), 131.9 (C-9a), 130.3 (C-5a), 127.7 (C-4′), 126.0 (C-6), 125.8 (C-9), 125.8 (C-5′), 122.4 (C-2′), 118.0 (C-10a), 101.6 (C-11a), 66.1 (C-3), 29.7 (C-11). HRMS (ESI): Found m/z 350.0484 [M + H]$^+$, calcd. for [C$_{19}$H$_{12}$NO$_4$S]$^+$: 350.0482.

11-(Furan-3-yl)-4,11-dihydrobenzo[*g*]furo[3,4-*b*]quinolin-1,5,10(3*H*)-trione (13b). Yield 83 mg (25% – approach A), 207 mg (62% – approach B), yellow-brown solid, mp. 345–346 °C. IR (KBr) ν_{max}/cm^{-1} 3199, 3118, 2961, 2927, 2857, 1712, 1658, 1628, 1604, 1590, 1503, 1396, 1357, 1335, 1303, 1194, 1071, 1014, 934, 874, 794, 727. ^{1}H NMR (DMSO-d_6, 600 MHz): δ 10.57 (1H, s, –NH), 8.06 (1H, dd, J = 1.2, 7.2 Hz, H-6), 7.93 (1H, dd, J = 1.2, 7.2 Hz, H-9), 7.86 (1H, td, J = 1.2, 7.2 Hz, H-8), 7.82 (1H, td, J = 1.2, 7.2 Hz, H-7), 7.49 (1H, t, J = 1.2 Hz), 7.47 (1H, t, J = 0.6 Hz), 6.40 (1H, dd, J = 0.6, 1.8 Hz), 4.98 (1H, d, J = 16.2 Hz, H^a-3), 4.94 (1H, s, H-11), 4.87 (1H, dd, J = 1.2, 16.2 Hz, H^b-3). ^{13}C NMR (DMSO-d_6, 125 MHz) δ 182.1 (C-10), 179.5 (C-5), 171.2 (C-1), 156.3 (C-3a), 143.0, 140.2, 139.2 (C4a), 134.9 (C8), 133.3 (C-7), 131.9 (C-9a), 130.2 (C-5a), 128.5, 125.9 (C6), 125.7 (C9), 117.6 (C-10a), 110.5, 101.0 (C-11a), 66.1 (C-3), 25.3 (C-11). HRMS (ESI): Found m/z 334.0693 [M + H]$^+$, calcd. for [C$_{19}$H$_{12}$NO$_5$]$^+$: 334.0710.

11-(Furan-2-yl)-4,11-dihydrobenzo[*g*]furo[3,4-*b*]quinolin-1,5,10(3*H*)-trione (13c). Yield 67 mg (20% – approach A), 200 mg (60% – approach B), orange solid, mp. 304–305 °C. IR (KBr) ν_{max}/cm^{-1} 3202, 3153, 2965, 2932, 1716, 1659, 1631, 1604, 1590, 1504, 1396, 1352, 1335, 1303, 1195, 1070, 1014, 933, 727. ^{1}H NMR (DMSO-d_6, 600 MHz): δ 10.70 (1H, s, NH), 8.06 (1H, dd, J = 1.2, 7.2 Hz, H-6), 7.96 (1H, dd, J = 1.2, 7.2 Hz, H-9), 7.87 (1H, td, J = 1.2, 7.2 Hz, H-8), 7.83 (1H, td, J = 1.2, 7.2 Hz, H-7), 7.46 (1H, dd, J = 0.6, 1.8 Hz), 6.32 (1H, q, J = 1.8 Hz), 6.19 (1H, d, J = 3.0 Hz), 5.14 (1H, s, H-11), 4.99 (1H, d, J = 16.8 Hz, H^a-3), 4.88 (1H, dd, J = 1.2, 16.8 Hz, H^b-3). ^{13}C NMR (DMSO-d_6, 125 MHz) δ 182.0, 179.5, 170.9, 156.6, 155.5, 141.9, 139.3, 135.1, 133.5, 131.8, 130.1, 126.1, 125.8, 115.9, 110.7, 106.6, 99.6, 66.1, 28.5. Found m/z 356.0513 [M + Na]$^+$, calcd. for [C$_{19}$H$_{11}$NNaO$_4$]$^+$: 356.0529.

11-(5-Bromofuran-2-yl)-4,11-dihydrobenzo[*g*]furo[3,4-*b*]quinolin-1,5,10(3*H*)-trione (13d). Yield 82 mg (20% – approach A), 256 mg (62% – approach B), orange-yellow solid, mp. 371–372 °C. IR (KBr) ν_{max}/cm^{-1} 3249, 1726, 1662, 1599, 1592, 1499, 1476, 1459, 1439, 1400, 1332, 1298, 1192, 1159, 1134, 1114, 1068, 1012, 960, 926, 779, 727. ^{1}H NMR (DMSO-d_6, 600 MHz): δ 10.74 (1H, s, NH), 8.06 (1H, dd, J = 0.8, 7.8 Hz, H-6), 7.96 (1H, dd, J = 1.2, 7.8 Hz, H-9), 7.87 (1H, td, J = 1.2, 7.8 Hz, H-8), 7.83 (1H, td, J = 1.8, 7.8 Hz, H-7), 6.42 (1H, d, J = 3.0 Hz), 6.28 (1H, d, J = 3.0 Hz), 5.11 (1H, s, H-11), 5.02 (1H, d, J = 16.8 Hz, H^a-3), 4.91 (1H, dd, J = 1.2, 16.8 Hz, H^b-3). ^{13}C NMR (DMSO-d_6, 125 MHz) δ 181.9, 179.4, 170.8, 158.0, 156.6, 139.5, 135.0, 133.5, 131.7, 130.2, 126.1, 125.8, 119.6, 115.2, 112.7, 109.8, 99.1, 66.2, 28.9. Found m/z 411.9832 and 413.9772 [M + H]$^+$, calcd. for [C$_{19}$H$_{11}$BrNO$_5$]$^+$: 411.9816 and 413.9795.

11-(Benzo[*b*]thiophen-3-yl)-4,11-dihydrobenzo[*g*]furo[3,4-*b*]quinolin-1,5,10(3*H*)-trione (13e). Yield 132 mg (33% – approach A), 279 mg (70% – approach B), red-brown solid, mp. 295–296 °C. IR (KBr) ν_{max}/cm^{-1} 3445, 3212, 3070, 2923, 2853, 1728, 1661, 1595, 1501, 1397, 1332, 1299, 1194, 1135, 1068, 1010, 922, 786, 762, 722. ^{1}H NMR (DMSO-d_6, 600 MHz): δ 10.72 (1H, s, NH), 8.24 (1H, d, J = 7.8 Hz), 8.08–8.06 (1H, m), 7.91 (1H, d, J = 7.8 Hz), 7.84–7.79 (3H, m), 7.55 (1H, s), 7.46 (1H, td, J = 1.2, 7.8 Hz), 7.38 (1H, td, J = 0.6, 7.8 Hz), 5.40 (1H, s), 4.97 (1H, d, J = 16.8 Hz), 4.91 (1H, d, J = 16.8 Hz). ^{13}C NMR (DMSO-d_6, 125 MHz) δ 182.0, 179.6, 171.1, 155.6, 141.21, 139.4, 139.2, 137.5, 134.8, 133.4, 131.8, 130.3, 126.4, 126.0, 125.7, 124.3, 124.0, 122.8, 122.5, 118.3, 102.0, 66.1, 27.9. HRMS (ESI): Found m/z 422.0429 [M + Na]$^+$, calcd. for [C$_{23}$H$_{13}$NNaO$_4$S]$^+$: 422.0458.

11-(Benzofuran-3-yl)-4,11-dihydrobenzo[*g*]furo[3,4-*b*]quinolin-1,5,10(3*H*)-trione (13f). Yield 123 mg (32% – approach A), 261 mg (68% – approach B), brown solid, mp. 295–296 °C. IR (KBr) ν_{max}/cm^{-1} 3215, 3097, 1749, 1734, 1664, 1640, 1597, 1506, 1451, 1399, 1341, 1301, 1196, 1110, 1066, 1009, 750, 725. ^{1}H NMR (DMSO-d_6, 600 MHz): δ 10.77 (1H, s), 8.08–8.05 (1H, m), 7.91 (1H, s), 7.90–7.89 (1H, m), 7.83 (1H, td, J = 1.8, 7.2 Hz), 7.80 (1H, td, J = 1.8, 7.2 Hz), 7.78 (1H, d, J = 1.2, 6.6 Hz), 7.50 (1H, d, J = 1.2, 7.2 Hz), 7.28 (1H, td, J = 1.8, 7.2 Hz), 7.26 (1H, td, J = 1.8, 7.2 Hz), 5.24 (1H, s), 4.99 (1H, d, J = 16.8 Hz), 4.92 (1H, dd, J = 1.2, 16.8 Hz), 3.73 (3H, s). ^{13}C NMR (DMSO-d_6, 125 MHz) δ 182.1, 179.5, 171.1, 156.4, 154.7, 144.4, 139.5, 134.9, 133.4, 131.9, 130.3, 126.3, 126.0, 125.7, 124.2, 123.9, 122.7, 120.3, 117.1, 111.2, 100.9, 66.1, 24.6. HRMS (ESI): Found m/z 384.0846 [M + H]$^+$, calcd. for [C$_{23}$H$_{14}$NO$_5$]$^+$: 384.0866.

11-(Benzo[*b*]thiophen-2-yl)-4,11-dihydrobenzo[*g*]furo[3,4-*b*]quinolin-1,5,10(3*H*)-trione (13g). Yield 132 mg (33% – approach A), 276 mg (69% – approach B), red-brown solid, mp. 302–303 °C. IR (KBr) ν_{max}/cm^{-1} 3466, 3050, 2924, 2853, 2263, 2126, 1773, 1740, 1667, 1637, 1591, 1495, 1431, 1394, 1341, 1296, 1192, 1157, 1137, 1066, 999, 927, 822, 788, 770, 748, 719. ^{1}H NMR (DMSO-d_6, 600 MHz): δ 10.84 (1H, s), 8.08 (1H, dd, J = 1.2, 7.2 Hz), 7.97 (1H, d, J = 7.2 Hz), 7.87 (1H, td, J = 1.2, 7.2 Hz), 7.85–7.81 (2H, m), 7.71 (1H, d, J = 7.8 Hz), 7.30 (1H, d, J = 1.2, 7.2 Hz), 7.25 (1H, d, J = 1.2, 8.4 Hz), 7.24 (1H, s), 5.38 (1H, s), 5.06 (1H, d, J = 16.2 Hz), 4.96 (1H, dd, J = 1.2, 16.2 Hz). ^{13}C NMR (DMSO-d_6, 125 MHz) δ 182.0, 179.4, 170.9, 156.5, 148.1, 139.4, 139.0, 138.9, 135.0, 133.5, 131.8, 130.2, 126.1, 125.9, 124.3, 124.0, 123.4, 122.3, 121.7, 117.2, 100.9, 66.2, 30.3. HRMS (ESI): Found m/z 400.0623 [M + H]$^+$, calcd. for [C$_{23}$H$_{14}$NO$_4$S]$^+$: 400.0638.

11-(2-Chlorothiazol-5-yl)-4,11-dihydrobenzo[*g*]furo[3,4-*b*]quinolin-1,5,10(3*H*)-trione (13h). Yield 108 mg (28% – approach A), 246 mg (64% – approach B), yellow-brown solid, mp. 383–384 °C. IR (KBr) ν_{max}/cm^{-1} 3341, 3092, 2922, 2852, 1774, 1734, 1660, 1602, 1525, 1507, 1478, 1443, 1414, 1397, 1335, 1300, 1267, 1240, 1199, 1159, 1140, 1044, 1019, 927, 878, 826, 776, 721, 705. ^{1}H NMR (DMSO-d_6, 600 MHz): δ 10.86 (1H, s), 8.06 (1H, dd, $J = 1.2, 7.8$ Hz), 7.99 (1H, dd, $J = 1.2, 7.8$ Hz), 7.88 (1H, td, $J = 1.2, 7.8$ Hz), 7.83 (1H, td, $J = 1.2, 7.8$ Hz), 7.48 (1H, d, $J = 0.6$ Hz), 5.29 (1H, s), 5.06 (1H, d, $J = 16.8$ Hz), 4.94 (1H, dd, $J = 1.2, 16.8$ Hz). ^{13}C NMR (DMSO-d_6, 125 MHz) δ 182.1, 179.3, 170.9, 169.7, 157.1, 143.9, 139.7, 139.5, 135.1, 133.6, 131.7, 130.3, 127.0, 125.9, 116.3, 99.9, 66.4, 27.7. HRMS (ESI): Found *m/z* 385.0026 [M + H]$^+$, calcd. for $[C_{18}H_{10}ClN_2O_4S]^+$: 385.0044.

11-(1,5-Dimethyl-1*H*-pyrazol-4-yl)-4,11-dihydrobenzo[*g*]furo[3,4-*b*]quinolin-1,5,10(3*H*)-trione (13i). Yield 98 mg (27% – approach A), 228 mg (63% – approach B), red-brown solid, mp. 262–263 °C. IR (KBr) ν_{max}/cm^{-1} 3439, 3290, 3163, 3077, 2925, 2854, 1722, 1660, 1596, 1490, 1428, 1393, 1331, 1298, 1267, 1191, 1134, 1108, 1065, 1037, 1011, 929, 884, 828, 792, 723. ^{1}H NMR (DMSO-d_6, 600 MHz): δ 10.52 (1H, s), 8.04 (1H, dd, $J = 1.2, 7.8$ Hz), 7.89 (1H, dd, $J = 1.2, 7.8$ Hz), 7.82 (1H, td, $J = 1.2, 7.8$ Hz), 7.79 (1H, td, $J = 1.2, 7.8$ Hz), 7.11 (1H, s), 4.94 (1H, d, $J = 16.2$ Hz), 4.85 (1H, dd, $J = 1.2, 16.2$ Hz), 4.79 (1H, s), 3.63 (3H, s), 2.30 (3H, s). ^{13}C NMR (DMSO-d_6, 150 MHz) δ 182.2, 179.7, 171.3, 155.3, 138.6, 137.2, 134.9, 134.7, 133.3, 131.9, 130.2, 126.0, 125.7, 122.4, 118.5, 102.0, 66.0, 36.0, 24.7, 9.1. HRMS (ESI): Found *m/z* 362.1118 [M + H]$^+$, calcd. for $[C_{20}H_{16}N_3O_4]^+$: 362.1135.

11-(1H-pyrazol-5-yl)-4,11-dihydrobenzo[*g*]furo[3,4-*b*]quinolin-1,5,10(3*H*)-trione (13j). Yield 67 mg (20% – approach A), 203 mg (61% – approach B), pink-red solid, mp. 310–311 °C. IR (KBr) ν_{max}/cm^{-1} 3337, 3249, 3207, 3148, 2960, 2927, 1725, 1664, 1630, 1590, 1499, 1398, 1354, 1304, 1199, 1167, 1054, 1011, 933, 784725. ^{1}H NMR (DMSO-d_6, 600 MHz): δ 12.39 (1H, br. s, NH), 10.55 (1H, s), 8.05 (1H, d, $J = 7.2$ Hz), 7.94 (1H, d, $J = 7.2$ Hz), 7.86 (1H, t, $J = 7.2$ Hz), 7.81 (1H, t, $J = 7.2$ Hz), 7.52 (1H, br. s), 6.13 (1H, br. s), 5.11 (1H, br. s), 4.93 (1H, d, $J = 16.8$ Hz), 4.87 (1H, d, $J = 16.8$ Hz). ^{13}C NMR (DMSO-d_6, 125 MHz) δ 182.1, 179.6, 171.2, 156.0, 135.0, 133.4, 131.9, 130.1, 126.0, 125.8, 103.2, 66.0, 29.8. HRMS (ESI): Found *m/z* 334.0808 [M + H]$^+$, calcd. for $[C_{18}H_{12}N_3O_4]^+$: 334.0822.

11-(2-Methoxypyridin-4-yl)-4,11-dihydrobenzo[*g*]furo[3,4-*b*]quinolin-1,5,10(3*H*)-trione (13k). Yield 127 mg (34% – approach A), 277 mg (74% – approach B), red-brown solid, mp. 245–246 °C. IR (KBr) ν_{max}/cm^{-1} 3455, 3044, 3014, 2984, 2941, 2893, 2740, 1739, 1665, 1630, 1601, 1561, 1505, 1478, 1396, 1341, 1300, 1192, 1167, 1147, 1068, 1045, 1021, 1004, 940, 786, 728. ^{1}H NMR (DMSO-d_6, 600 MHz): δ 10.69 (1H, s), 8.07 (1H, dd, $J = 1.2, 7.2$ Hz), 8.04 (1H, dd, $J = 1.2, 5.4$ Hz), 7.90 (1H, dd, $J = 1.2, 7.2$ Hz), 7.86–7.81 (2H, m), 6.99 (1H, dd, $J = 1.2, 5.4$ Hz), 6.74 (1H, s), 4.99 (1H, s), 4.98 (1H, d, $J = 16.8$ Hz), 4.90 (1H, dd, $J = 16.8$ Hz), 3.79 (3H, s). ^{13}C NMR (DMSO-d_6, 125 MHz) δ 182.0, 179.3, 170.9, 163.8, 156.5, 155.2, 146.6, 140.1, 134.8, 133.4, 131.8, 130.3, 126.0, 125.7, 117.1, 116.9, 109.7, 100.8, 66.2, 53.0, 34.7. HRMS (ESI): Found *m/z* 375.0960 [M + H]$^+$, calcd. for $[C_{21}H_{15}N_2O_5]^+$: 375.0976.

11-(3-Fluoropyridin-2-yl)-4,11-dihydrobenzo[*g*]furo[3,4-*b*]quinolin-1,5,10(3*H*)-trione (13l). Yield 116 mg (32% – approach A), 261 mg (72% – approach B), grey-red solid, mp. 288–289 °C. IR (KBr) ν_{max}/cm^{-1} 3349, 3221, 3081, 2928, 2857, 1747, 1671, 1660, 1630, 1607, 1497, 1442, 1397, 1343, 1303, 1194, 1066, 1005, 803, 724. ^{1}H NMR (DMSO-d_6, 600 MHz): δ 10.48 (1H, s), 8.25–8.23 (1H, m), 8.07 (1H, dd, $J = 2.4, 8.4$ Hz), 7.88–7.84 (1H, m), 7.83–7.78 (2H, m), 7.63–7.58 (1H, m), 7.27 (1H, quint, $J = 5.4$ Hz), 5.51 (1H, s), 4.92 (2H, t, $J = 16.2$ Hz). ^{13}C NMR (DMSO-d_6, 125 MHz) δ 181.6, 179.3, 170.4, 156.4, 155.3 (1C, d, $J = 256.3$ Hz), 149.8 (1C, d, $J = 15$ Hz), 145.0 (1C, d, $J = 6.3$ Hz), 139.9, 134.8, 133.2, 131.5, 129.8, 125.8, 125.5, 123.5 (1H, d, $J = 3.8$ Hz), 122.4 (1H, d, $J = 20$ Hz), 118.0, 100.3, 65.9, 30.7. HRMS (ESI): Found *m/z* 363.0760 [M + H]$^+$, calcd. for $[C_{20}H_{12}FN_2O_4]^+$: 363.0776.

11-(2-Methoxy-5-(trifluoromethyl)pyridin-3-yl)-4,11-dihydrobenzo[*g*]furo[3,4-*b*]quinolin-1,5,10(3*H*)-trione (13m). Yield 146 mg (33% – approach A), 318 mg (72% – approach B), yellow-orange solid, mp. 289–290 °C. IR (KBr) ν_{max}/cm^{-1} 3285, 3079, 3027, 2997, 2950, 1725, 1663, 1603, 1577, 1495, 1437, 1400, 1322, 1297, 1246, 1195, 1144, 1116, 1093, 1072, 1015, 940, 724. ^{1}H NMR (DMSO-d_6, 600 MHz): δ 10.63 (1H, s), 8.41 (1H, d, $J = 1.2$ Hz), 8.05 (1H, dd, $J = 1.2, 7.2$ Hz), 8.00 (1H, d, $J = 2.4$ Hz), 7.85 (1H, dd, $J = 1.2, 7.2$ Hz), 7.84–7.78 (2H, m), 5.34 (1H, s), 4.95 (1H, d, $J = 16.2$ Hz), 4.89 (1H, dd, $J = 0.6, 16.2$ Hz), 3.96 (3H, s). ^{13}C NMR (DMSO-d_6, 150 MHz) δ 181.9, 179.4, 170.7, 163.2, 156.8, 142.9 (1C, d, $J = 4.5$ Hz), 140.5, 135.3, 134.9, 133.3, 131.8, 130.1, 127.3, 125.9, 125.7, 124.1 (1C, q, $J = 270$ Hz), 118.8 (1C, q, $J = 31.5$ Hz), 117.0, 100.2, 66.0, 54.2, 30.6. HRMS (ESI): Found *m/z* 443.0836 [M + H]$^+$, calcd. for $[C_{22}H_{14}F_3N_2O_5]^+$: 443.0849.

MTT assay

The investigated cancer cell lines were purchased from the American Type Culture Collection (ATCC, USA). The cytotoxicity of the newly synthesized series of compounds was studied against non-small lung (A549, CCL-185™), epidermoid carcinoma (KB, CCL-17™), breast (MCF7, HTB-22™), hepatocellular carcinoma (HepG2, HB-8065™), cancer cells, and human embryonic kidney (Hek-293, CRL-1573™) cells, which were cultured in DMEM (Dulbeccos Modified Eagle Medium) medium, supplemented with 10% fetal bovine serum, 100 U ml^{-1} penicillin, and 100 μg mL^{-1} streptomycin, at 37 °C in humidified atmosphere (95% air and 5% CO_2). Solutions of compounds **13a–m** in DMSO at different concentratrions (1.00, 0.25, 0.0625, and 0.0156 μg mL^{-1}) were added to human cancer cell lines (3×10^4 cells per ml). After 3 days-incubation, 10 μl solution of 5 mg mL^{-1} MTT in sodium phosphate buffer (PBS, 0.1 M, pH 7.4) was then supplemented, the cells were incubated at 37 °C for 4 h, and then removed medium. The obtained formazan crystals were dissolved by DMSO (150 μl). A Biotek Epoch 2 microplate reader was used to measure the absorbance of the solutions at 540 nm.[63–65]

Molecular docking study

Molecular docking studies were performed for all the synthesized compounds against the tubulin target. To do so, the tubulin-colchicine complex (PDB ID: 4O2B) was taken from the Protein Data Bank.[52] They were prepared for docking assays following the standard protocol implemented into ICM Pro (x64) software.[44,66] The chains α and β tubulin were retained, followed by deleting all the water molecules, optimizing all hydrogens and optimizing HisProAsnGlnCys, setting MMFF forcefield, and predicting the binding site of Colchicine by using ICMpocketfinder.[67] The 2D structures of synthesized compounds **13a–13m** were generated using ChemDraw 20.1.1, then imported to ICM Pro software and convert to 3D conformations for docking. Before docking synthesized compounds, the co-crystallized ligand colchicine was removed, and redocked into the binding site of Tubulin. Conformational sampling is based on the biased probability Monte Carlo (BPMC) procedure. The ICM scoring function is a GBSA/MM-type,[66] which is weighted according to the following parameters (i) internal force-field energy of the ligand, (ii) entropy loss of the ligand between bound and unbound states, (iii) ligand-receptor hydrogen bond interactions, (iv) polar and non-polar solvation energy differences between bound and unbound states, (v) electrostatic energy, (vi) hydrophobic energy, and (vii) hydrogen bond donor or acceptor desolvation. The binding energy (kcal mol^{-1}) is calculated *via* equation: $\Delta G = \Delta E_{IntFF} + T\Delta S_{Tor} + \alpha_1\Delta E_{HBond} + \alpha_2\Delta E_{HBDesol} + \alpha_3\Delta E_{SolEl} + \alpha_4\Delta E_{HPhob} + \alpha_5 Q_{Size}$.[66] For each ligand, 50 conformations were generated, and the conformations with better binding scores and key interactions similar to colchicine were selected for further studies. The docking results were then visualized using BIOVIA Discovery Studio Visualizer 2021.

Physicochemical and pharmacokinetic properties prediction

Calculations of the physicochemical parameters of synthesized compounds relevant to ADME were performed using SwissAMDE, a free online cheminformatics tool.[57] Computed parameters are related to the evaluation of drug-likeness, lead-likeness characteristics such as Lipinski, Veber, Goshe, Egan, and Muegge rules.[68] Additionally, their toxicity was also predicted by another web-based tool – ADMETlab 2.0.[62,69] The parameters can be rapidly determined by easily inputting the SMILES codes of the compounds into the website.

Conclusions

A series of new heterocyclic hybrid compounds of 4-azapodophyllotoxin were successfully synthesized *via* microwave-assisted multicomponent reactions. The efficient synthesis of novel hybrid compounds has been expected to facilitate the discovery of numerous classes of bioactive heterocyclic compounds. Obviously, the *in vitro* cytotoxic assessment and molecular docking study revealed that all products showed cytotoxic activity and they are all capable of binding to the active site of colchicine in tubulin. Compounds **13a** (HetAr = thiophen-3-yl), and **13d** (HetAr = 5-bromofuran-2-yl) displayed high cytotoxic selectivity for A549 and HepG2 cancer cell lines when compared to the other cancer cell lines and low toxicity to normal Hek-293 cell line with $IC_{50} = 22.90 \pm 2.18$ and 37.12 ± 3.30 μM, respectively. The most active compound **13k** containing 2-methoxypyridin-4-yl group exhibited significant cytotoxicity against human lung adenocarcinoma cells, human mouth epidermal carcinoma cells, and human hepatocellular carcinoma cells with IC_{50} ranging from 0.23 to 0.27 μM. Compound **13h** (HetAr = 2-chlorothiazol-5-yl) displayed the highest toxicity against A549 cells with $IC_{50} = 0.16 \pm 0.02$ μM. Notably, compounds **13h,k**, which have strong binding energy with the active site of tubulin at −17.86, and −18.05 kcal mol^{-1}, respectively, provided suitable physicochemical and ADMET profiles to be considered as good anticancer compounds. Taken together, these potent cytotoxic compounds have potential for investigation into the anticancer activity.

Author contributions

Ha Thanh Nguyen: project administration: conceptual design; writing – original draft. Ket Tran Van, and Phuong Hoang Thi: investigation: synthesis of compounds. Julien Braire and Quynh Giang Nguyen Thi: investigation: characterisation of compounds. Tu Anh Le Thi and Giang Le-Nhat-Thuy: investigation: biological evaluation of compounds. Tuyet Anh Dang Thi and Doan Vu Ngoc: investigation: revised draft. Hai Pham-The and Tuan Anh Nguyen: investigation: molecular docking studies. Tuyen Van Nguyen: supervision: conceptual design; writing – review & editing.

Conflicts of interest

There are no conflicts to declare.

Acknowledgements

The authors are indebted to National Foundation for Science and Technology Development (NAFOSTED) Grant number: 104.01-2021.50 for financial support. Ha Thanh Nguyen was also funded by the Postdoctoral Scholarship Programme of Vingroup Innovation Foundation (VINIF), code VINIF.2023.STS.29.

Notes and references

1 G. Le-Nhat-Thuy, T. A. Dang Thi, Q. G. Nguyen Thi, P. Hoang Thi, T. A. Nguyen, H. T. Nguyen, T. H. Nguyen Thi, H. S. Nguyen and T. V. Nguyen, Synthesis and biological evaluation of novel benzo[a]pyridazino[3,4-c]phenazine derivatives, *Bioorg. Med. Chem. Lett.*, 2021, **43**, 128054.
2 V. Bhardwaj, M. N. Noolvi, S. Jalhan and H. M. Patel, Synthesis, and antimicrobial evaluation of new pyridine imidazo [2,1b]-1,3,4-thiadiazole derivatives, *J. Saudi Chem. Soc.*, 2016, **20**, S406–S410.
3 V. Kamat, R. Santosh, B. Poojary, S. P. Nayak, B. K. Kumar, M. Sankaranarayanan, Faheem, S. Khanapure, D. A. Barretto and S. K. Vootla, Pyridine- and thiazole-based hydrazides with promising anti-inflammatory and antimicrobial activities along with their in silico studies, *ACS Omega*, 2020, **5**, 25228–25239.
4 H. T. Nguyen, T. H. Nguyen Thi, J. Braire, T. A. Dang Thi and T. Nguyen Van, Microwave-assisted multicomponent synthesis of new 6-arylated 5-hydroxy-benzo[*a*]phenazine derivatives and their potential anti-inflammatory activity, *ChemistrySelect*, 2023, **8**, e202204376.

5 H. T. Nguyen, A. N. Tuan, T. A. D. Thi, K. T. Van, G. Le-Nhat-Thuy, P. H. Thi, Q. G. N. Thi, C. B. Thi, H. T. Quang and T. Van Nguyen, Synthesis, *in vitro* α-glucosidase, and acetylcholinesterase inhibitory activities of novel indol-fused pyrano[2,3-*d*]pyrimidine compounds, *Bioorg. Med. Chem. Lett.*, 2023, 129566.

6 H. T. Nguyen, G. Le-Nhat-Thuy, P. H. Thi, Q. G. N. Thi, T. A. Nguyen, T. H. N. Thi, T. A. D. Thi and T. V. Nguyen, Microwave-Assisted Three-Component Synthesis of Novel N-Arylated-Dihydrobenzo[g]quinoline-5,10-Diones and Their Potential Cytotoxic Activity, *Chem. Biodiversity*, 2022, **19**, e202200359.

7 N. T. Dung, L. N. T. Giang, P. H. Thu, N. H. Thuong, D. T. Tuyet Anh, L. Q. Tan, N. H. Thanh, L. T. T. Anh, N. T. Anh, B. L. Giang, N. V. Tuyen and P. V. Kiem, Synthesis and cytotoxic evaluation of carboxylic acid-functionalized indenoisoquinolines, *Nat. Prod. Commun.*, 2019, **14**, 1934578x1984978.

8 A. A. Abbas and K. M. Dawood, Anticancer therapeutic potential of benzofuran scaffolds, *RSC Adv.*, 2023, **13**, 11096–11120.

9 T. A. Dang Thi, T. H. Vu Thi, H. Thi Phuong, T. Ha Nguyen, C. Pham The, C. Vu Duc, Y. Depetter, T. Van Nguyen and M. D'hooghe, Synthesis and anticancer properties of new (dihydro)pyranonaphthoquinones and their epoxy analogs, *Bioorg. Med. Chem. Lett.*, 2015, **25**, 3355–3358.

10 M. Ashraf-Uz-Zaman, X. Li, Y. Yao, C. B. Mishra, B. K. Moku and Y. Song, Quinazolinone Compounds Have Potent Antiviral Activity against Zika and Dengue Virus, *J. Med. Chem.*, 2023, **66**, 10746–10760.

11 R. J. Obaid, N. Naeem, E. U. Mughal, M. M. Al-Rooqi, A. Sadiq, R. S. Jassas, Z. Moussa and S. A. Ahmed, Inhibitory potential of nitrogen, oxygen and sulfur containing heterocyclic scaffolds against acetylcholinesterase and butyrylcholinesterase, *RSC Adv.*, 2022, **12**, 19764–19855.

12 X. Li and Y. Song, Structure and function of SARS-CoV and SARS-CoV-2 main proteases and their inhibition: A comprehensive review, *Eur. J. Med. Chem.*, 2023, **260**, 115772.

13 C. H. Takimoto and A. Awada, Safety and anti-tumor activity of sorafenib (Nexavar®) in combination with other anti-cancer agents: a review of clinical trials, *Cancer Chemother. Pharmacol.*, 2008, **61**, 535–548.

14 F. Fondevila, C. Méndez-Blanco, P. Fernández-Palanca, J. González-Gallego and J. L. Mauriz, Anti-tumoral activity of single and combined regorafenib treatments in preclinical models of liver and gastrointestinal cancers, *Exp. Mol. Med.*, 2019, **51**, 1–15.

15 K. V. M. Huber, E. Salah, B. Radic, M. Gridling, J. M. Elkins, A. Stukalov, A.-S. Jemth, C. Göktürk, K. Sanjiv, K. Strömberg, T. Pham, U. W. Berglund, J. Colinge, K. L. Bennett, J. I. Loizou, T. Helleday, S. Knapp and G. Superti-Furga, Stereospecific targeting of MTH1 by (S)-crizotinib as an anticancer strategy, *Nature*, 2014, **508**, 222–227.

16 A. Srirangam, M. Milani, R. Mitra, Z. Guo, M. Rodriguez, H. Kathuria, S. Fukuda, A. Rizzardi, S. Schmechel, D. G. Skalnik, L. M. Pelus and D. A. Potter, The human immunodeficiency virus protease inhibitor ritonavir inhibits lung cancer cells, in part, by inhibition of survivin, *J. Thorac. Oncol.*, 2011, **6**, 661–670.

17 R. Batchu, O. Gruzdyn, C. Bryant, A. Qazi, S. Kumar, S. Chamala, S. Kung, R. Sanka, U. Puttagunta, D. Weaver and S. Gruber, Ritonavir-mediated induction of apoptosis in pancreatic cancer occurs via the rb/e2f-1 and akt pathways, *Pharmaceuticals*, 2014, **7**, 46–57.

18 S. J. Connolly, Evidence-based analysis of amiodarone efficacy and safety, *Circulation*, 1999, **100**, 2025–2034.

19 A. T. Lenis, P. M. Lec, K. Chamie and M. MSHS, Bladder Cancer: A Review, *JAMA*, 2020, **324**, 1980–1991.

20 M. Belcourt, P. Penketh, W. Hodnick, D. Johnson, D. Sherman, S. Rockwell and A. Sartorelli, Mitomycin resistance in mammalian cells expressing the bacterial mitomycin C resistance protein MCRA, *Proc. Natl. Acad. Sci. U.S.A.*, 1999, **96**, 10489–10494.

21 T. Nguyen Van, G. Verniest, S. Claessens and N. De Kimpe, Total synthesis of four naturally occurring 2-azaanthraquinone antibiotics, 6-deoxy-8-methylbostrycoidin, 6-deoxybostrycoidin, 7-O-demethyl-6-deoxybostrycoidin and scorpinone, *Tetrahedron*, 2005, **61**, 2295–2300.

22 H. T. Nguyen, H. Nguyen Van, P. Hoang Thi, T. A. D. Thi, G. Le-Nhat-Thuy, Q. G. Nguyen Thi, A. N. Tuan, C. Ba Thi, H. Tran Quang and T. Van Nguyen, Synthesis and cytotoxic evaluation of new fluoro and trifluoromethyl substituents containing chromeno[2,3- *d*]pyrimidines, *ChemistrySelect*, 2023, **8**, e202300227.

23 N. H. Thanh, H. T. Phuong, L. N. T. Giang, N. T. Q. Giang, N. T. T. Ha, D. T. T. Anh, V. D. Cuong, N. Van Tuyen and P. Van Kiem, 4-(Dimethylamino)pyridine as an efficient catalyst for one-pot synthesis of 1,4-pyranonaphthoquinone derivatives *via* microwave-assisted sequential three component reaction in green solvent, *Nat. Prod. Commun.*, 2021, **16**, 1934578X2110539.

24 N. H. Thanh, N. T. Q. Giang, N. V. Ha, H. T. Phuong, L. N. Thuy Giang, N. T. Anh, B. T. Cham, L. D. Huy, D. T. T. Anh, P. Van Kiem and N. V. Tuyen, Synthesis and evaluation of acetylcholinesterase inhibitory and cytotoxic activities of pyrano[2,3- *d*]pyrimidines, *Nat. Prod. Commun.*, 2023, **18**, 1934578X231201037.

25 M. M. Abdelshaheed, H. I. El Subbagh, M. A. Tantawy, R. T. Attia, K. M. Youssef and I. M. Fawzy, Discovery of new pyridine heterocyclic hybrids; design, synthesis, dynamic simulations, and *in vitro* and *in vivo* breast cancer biological assays, *RSC Adv.*, 2023, **13**, 15689–15703.

26 G. Le-Nhat-Thuy, T. V. Dinh, H. Pham-The, H. Nguyen Quang, N. Nguyen Thi, T. A. Dang Thi, P. Hoang Thi, T. A. Le Thi, H. T. Nguyen, P. Nguyen Thanh, T. Le Duc and T. V. Nguyen, Design, synthesis and evaluation of novel hybrids between 4-anilinoquinazolines and substituted triazoles as potent cytotoxic agents, *Bioorg. Med. Chem. Lett.*, 2018, **28**, 3741–3747.

27 T. A. Dang Thi, Y. Depetter, K. Mollet, H. Thi Phuong, D. Vu Ngoc, C. Pham The, H. Thanh Nguyen, T. H. Nguyen Thi, H. Huy Nguyen, M. D'hooghe and T. Van Nguyen,

Expedient stereoselective synthesis of new dihydropyrano- and dihydrofuranonaphthoquinones, *Tetrahedron Lett.*, 2015, **56**, 2422–2425.

28 G. Le-Nhat-Thuy, T. A. Dang Thi, P. Hoang Thi, Q. G. Nguyen Thi, H.-T. Nguyen, D. Vu Ngoc, T.-A. Nguyen and T. Van Nguyen, Multicomponent synthesis of novel 3-benzoyl-4h-benzo[g]chromene-5,10-dione derivatives, *Tetrahedron Lett.*, 2021, **75**, 153215.

29 I. Dine, E. Mulugeta, Y. Melaku and M. Belete, Recent advances in the synthesis of pharmaceutically active 4-quinolone and its analogues: a review, *RSC Adv.*, 2023, **13**, 8657–8682.

30 Y. You, Podophyllotoxin derivatives: current synthetic approaches for new anticancer agents, *Curr. Pharm. Des.*, 2005, **11**, 1695–1717.

31 N. Jeedimalla, M. Flint, L. Smith, A. Haces, D. Minond and S. P. Roche, Multicomponent assembly of 4-aza-podophyllotoxins: A fast entry to highly selective and potent anti-leukemic agents, *Eur. J. Med. Chem.*, 2015, **106**, 167–179.

32 I. V. Magedov, M. Manpadi, E. Rozhkova, N. M. Przheval'skii, S. Rogelj, S. T. Shors, W. F. A. Steelant, S. V. slambrouck and A. Kornienko, Structural simplification of bioactive natural products with multicomponent synthesis: Dihydropyridopyrazole analogues of podophyllotoxin, *Bioorg. Med. Chem. Lett.*, 2007, **17**, 1381–1385.

33 A. Kamal, P. Suresh, A. Mallareddy, B. A. Kumar, P. V. Reddy, P. Raju, J. R. Tamboli, T. B. Shaik, N. Jain and S. V. Kalivendi, Synthesis of a new 4-aza-2,3-didehydropodophyllotoxin analogues as potent cytotoxic and antimitotic agents, *Bioorg. Med. Chem.*, 2011, **19**, 2349–2358.

34 A. Kamal, J. R. Tamboli, V. L. Nayak, S. F. Adil, M. V. P. S. Vishnuvardhan and S. Ramakrishna, Synthesis of a terphenyl substituted 4-aza-2,3-didehydropodophyllotoxin analogues as inhibitors of tubulin polymerization and apoptosis inducers, *Bioorg. Med. Chem.*, 2014, **22**, 2714–2723.

35 M. N. Semenova, A. S. Kiselyov, D. V. Tsyganov, L. D. Konyushkin, S. I. Firgang, R. V. Semenov, O. R. Malyshev, M. M. Raihstat, F. Fuchs, A. Stielow, M. Lantow, A. A. Philchenkov, M. P. Zavelevich, N. S. Zefirov, S. A. Kuznetsov and V. V. Semenov, Polyalkoxybenzenes from plants. 5. parsley seed extract in synthesis of azapodophyllotoxins featuring strong tubulin destabilizing activity in the sea urchin embryo and cell culture assays, *J. Med. Chem.*, 2011, **54**, 7138–7149.

36 I. V. Magedov, M. Manpadi, S. Van slambrouck, W. F. A. Steelant, E. Rozhkova, N. M. Przheval'skii, S. Rogelj and A. Kornienko, Discovery and investigation of antiproliferative and apoptosis-inducing properties of new heterocyclic podophyllotoxin analogues accessible by a one-step multicomponent synthesis, *J. Med. Chem.*, 2007, **50**, 5183–5192.

37 R. Labruère, B. Gautier, M. Testud, J. Seguin, C. Lenoir, S. Desbène-Finck, P. Helissey, C. Garbay, G. G. Chabot, M. Vidal and S. Giorgi-Renault, Design, Synthesis, and biological evaluation of the first podophyllotoxin analogues as potential vascular-disrupting agents, *ChemMedChem*, 2010, **5**, 2016–2025.

38 N. H. Thanh, H. T. Phuong, L. T. Tu Anh, L. N. Thuy Giang, N. T. Quynh Giang, N. T. Anh, D. T. Tuyet Anh and P. Van Kiem, Synthesis and cytotoxic evaluation of fluoro and trifluoromethyl substituents containing novel naphthoquinone-fused podophyllotoxins, *Nat. Prod. Commun.*, 2022, **17**, 1934578X2211331.

39 F. Shi, X.-N. Zeng, G. Zhang, N. Ma, B. Jiang and S. Tu, Facile synthesis of new 4-aza-podophyllotoxin analogs via microwave-assisted multi-component reactions and evaluation of their cytotoxic activity, *Bioorg. Med. Chem. Lett.*, 2011, **21**, 7119–7123.

40 C. Shi, J. Wang, H. Chen and D. Shi, Regioselective synthesis and in vitro anticancer activity of 4-aza-podophyllotoxin derivatives catalyzed by l -proline, *J. Comb. Chem.*, 2010, **12**, 430–434.

41 N. H. Thanh, L. Q. Bao, H. Pham-The, D. T. T. Anh and P. Van Kiem, Synthesis, molecular docking, and cytotoxic evaluation of fluorinated podophyllotoxin derivatives, *Nat. Prod. Commun.*, 2023, **18**, 1934578X2311537.

42 X. Yang, C. Zhang and L. Wu, l -Proline catalyzed three-component synthesis of para-naphthoquinone–4-aza-podophyllotoxin hybrids as potent antitumor agents, *RSC Adv.*, 2015, **5**, 18945–18951.

43 Q. G. Nguyen Thi, G. Le-Nhat-Thuy, T. A. Dang Thi, P. Hoang Thi, A. Nguyen Tuan, T. H. Nguyen Thi, T. T. Nguyen, T. Nguyen Ha, H. Hoang Mai and T. V. Nguyen, Synthesis of novel potent cytotoxicy podophyllotoxin-naphthoquinone compounds via microwave-assited multicomponent domino reactions, *Bioorg. Med. Chem. Lett.*, 2021, **37**, 127841.

44 H. T. Nguyen, Q. G. Nguyen Thi, T. H. Nguyen Thi, P. H. Thi, G. Le-Nhat-Thuy, T. A. Dang Thi, B. Le-Quang, H. Pham-The and T. Van Nguyen, Synthesis and biological activity, and molecular modelling studies of potent cytotoxic podophyllotoxin-naphthoquinone compounds, *RSC Adv.*, 2022, **12**, 22004–22019.

45 H.-T. Nguyen, P. H. Thi, G. Le-Nhat-Thuy, Q. G. N. Thi, T. A. Nguyen, T. A. D. Thi and T. V. Nguyen, Synthesis of novel γ-butyrolactone-based phenazine compounds via microwave-assisted multicomponent domino reactions, *Chem. Heterocycl. Compd.*, 2022, **58**, 749–755.

46 H.-T. Nguyen, T. A. Dang Thi, P. Hoang Thi, G. Le-Nhat-Thuy, Q. G. Nguyen Thi, A. Nguyen Tuan, T. A. Le Thi and T. Van Nguyen, A new approach for the synthesis of novel naphthoquinone chalcone hybrid compounds, *Tetrahedron Lett.*, 2021, **81**, 153337.

47 H. T. Nguyen, T. H. Nguyen Thi, J. Braire, T. A. Dang Thi and T. Nguyen Van, Microwave-assisted multicomponent synthesis of new 6-arylated 5-hydroxy-benzo[*a*]phenazine derivatives and their potential anti-inflammatory activity, *ChemistrySelect*, 2023, **8**, e202204376.

48 B. Kesteleyn, T. N. Van and N. De Kimpe, Synthesis of 3-alkyl- and 3-aryl-2-aza-anthraquinones, *Tetrahedron*, 1999, **55**, 2091–2102.

49 N. Van Tuyen, B. Kesteleyn and N. De Kimpe, Synthesis of 2-alkoxymethyl-3-trifluoromethyl-1,4-naphthoquinones, *Tetrahedron*, 2002, **58**, 121–127.

50 R. A. Stanton, K. M. Gernert, J. H. Nettles and R. Aneja, Drugs that target dynamic microtubules: A new molecular perspective, *Med. Res. Rev.*, 2011, **31**, 443–481.

51 J. D. Loike and S. B. Horwitz, Effects of podophyllotoxin and VP-16-213 on microtubule assembly in vitro and nucleoside transport in HeLa cells, *Biochemistry*, 1976, **15**, 5435–5443.

52 A. E. Prota, F. Danel, F. Bachmann, K. Bargsten, R. M. Buey, J. Pohlmann, S. Reinelt, H. Lane and M. O. Steinmetz, The novel microtubule-destabilizing drug bal27862 binds to the colchicine site of tubulin with distinct effects on microtubule organization, *J. Mol. Biol.*, 2014, **426**, 1848–1860.

53 A. Massarotti, A. Coluccia, R. Silvestri, G. Sorba and A. Brancale, The tubulin colchicine domain: a molecular modeling perspective, *ChemMedChem*, 2012, **7**, 33–42.

54 W. Li, H. Sun, S. Xu, Z. Zhu and J. Xu, Tubulin inhibitors targeting the colchicine binding site: a perspective of privileged structures, *Future Med. Chem.*, 2017, **9**, 1765–1794.

55 H. Pham-The, M. Á. Cabrera-Pérez, N.-H. Nam, J. A. Castillo-Garit, B. Rasulev, H. Le-Thi-Thu and G. M. Casañola-Martin, In silico assessment of adme properties: advances in caco-2 cell monolayer permeability modeling, *Curr. Top. Med. Chem.*, 2019, **18**, 2209–2229.

56 H. Pham-The, I. González-Álvarez, M. Bermejo, T. Garrigues, H. Le-Thi-Thu and M. Á. Cabrera-Pérez, The use of rule-based and qspr approaches in adme profiling: a case study on caco-2 permeability, *Mol. Inf.*, 2013, **32**, 459–479.

57 A. Daina, O. Michielin and V. Zoete, SwissADME: a free web tool to evaluate pharmacokinetics, drug-likeness and medicinal chemistry friendliness of small molecules, *Sci. Rep.*, 2017, **7**, 42717.

58 H. Pham-The, T. Garrigues, M. Bermejo, I. González-Álvarez, M. C. Monteagudo and M. Á. Cabrera-Pérez, Provisional classification and *in silico* study of biopharmaceutical system based on caco-2 cell permeability and dose number, *Mol. Pharmaceutics*, 2013, **10**, 2445–2461.

59 A. Daina and V. Zoete, A BOILED-Egg to predict gastrointestinal absorption and brain penetration of small molecules, *ChemMedChem*, 2016, **11**, 1117–1121.

60 A. J. Castillo-Garit, M. G. Casanola-Martin, H. Le-Thi-Thu, H. Pham-The and J. S. Barigye, A simple method to predict blood–brain barrier permeability of drug- like compounds using classification trees, *Med. Chem.*, 2017, **13**, 664–669.

61 M. Á. Cabrera-Pérez and H. Pham-The, Computational modeling of human oral bioavailability: what will be next?, *Expert Opin. Drug Discovery*, 2018, **13**, 509–521.

62 G. Xiong, Z. Wu, J. Yi, L. Fu, Z. Yang, C. Hsieh, M. Yin, X. Zeng, C. Wu, A. Lu, X. Chen, T. Hou and D. Cao, ADMETlab 2.0: an integrated online platform for accurate and comprehensive predictions of ADMET properties, *Nucleic Acids Res.*, 2021, **49**, W5–W14.

63 P. T. Tham, P. T. Chinh, N. V. Tuyen, D. N. Bang, D. T. Van, V. T. Kien, H. T. Thanh, D. H. Quynh, V. D. Cuong, N. H. Thanh and A. Pérez-Encabo, Synthesis and cytotoxic evaluation of novel simplified plinabulin-quinoline derivatives, *Mendeleev Commun.*, 2021, **31**, 213–215.

64 H. T. Pham, G. Le-Nhat-Thuy, T. A. D. Thi, P. H. Thi, T. A. Nguyen, T. H. Nguyen, T. D. Nguyen, H. T. Ngo, T. A. Le and T. Van Nguyen, Synthesis and evaluation of the cytotoxicity of indeno[1,2-c]isoquinoline derivatives bearing ester functional group and 1,2,3-triazole moiety, *Chem. Heterocycl. Compd.*, 2020, **56**, 1167–1172.

65 T. Pham Thi, T. G. Le Nhat, T. Ngo Hanh, T. Luc Quang, C. Pham The, T. A. Dang Thi, H. T. Nguyen, T. H. Nguyen, P. Hoang Thi and T. Van Nguyen, Synthesis and cytotoxic evaluation of novel indenoisoquinoline-substituted triazole hybrids, *Bioorg. Med. Chem. Lett.*, 2016, **26**, 3652–3657.

66 M. A. C. Neves, M. Totrov and R. Abagyan, Docking and scoring with ICM: the benchmarking results and strategies for improvement, *J. Comput.-Aided Mol. Des.*, 2012, **26**, 675–686.

67 L. C. Huan, H. Pham-The, H. Le-Thi-Thu, T. P. Thao, D. N. Que, N.-T. Trang, P. T. Phuong Dung, M. Pyo, S.-B. Han, N. T. Thuan and N.-H. Nam, Exploration of some thiazolidine-2,4-dione and 2-oxoindoline derivatives incorporating 3,4,5-trimethoxybenzyl moiety as novel anticancer agents, *Lett. Drug Des. Discovery*, 2018, **15**, 375–387.

68 M. A. Cabrera-Perez, H. Pham-The, M. Bermejo, I. G. Alvarez, M. G. Alvarez and T. M. Garrigues, QSPR in oral bioavailability: specificity or integrality?, *Mini-Rev. Med. Chem.*, 2012, **12**, 534–550.

69 G. Xiong, Z. Wu, J. Yi, L. Fu, Z. Yang, C. Hsieh, M. Yin, X. Zeng, C. Wu, A. Lu, X. Chen, T. Hou and D. Cao, ADMETlab 2.0: An integrated online platform for accurate and comprehensive predictions of ADMET properties, *Nucleic Acids Res.*, 2021, **49**, W5–W14.